Cite this: DOI: 10.1039/xxxxxxxxxx

Electrokinetics of nanoparticle gel-electrophoresis

Reghan J. Hill[a*]

Received Date
Accepted Date

DOI: 10.1039/xxxxxxxxxx

www.rsc.org/journalname

Gel-electrophoresis has been demonstrated in recent decades to successfully sort a great variety of nanoparticles according to their size, charge, surface chemistry, and corona architecture. However, quantitative theoretical interpetations have been limited by the number and complexity of factors that influence particle migration. Theoretical models have been fragmented and incomplete with respect to their counterparts for free-solution electrophoresis. This paper unifies electrokinetic models that address complex nanoparticle corona architectures, corona and gel charge regulation (e.g., by the local pH), multi-component electrolytes, and non-linear electrostatics and relaxation effects. By comprehensively addressing the electrokinetic aspects of the more general gel-electrophoresis problem, in which short-ranged steric interactions are significant, a stage is set to better focus on the physicochemical and steric factors. In this manner, it is envisioned that noparticle gel-electrophoresis may eventually be advanced from a nanoparticle-characterization tool to one that explicitly probes the short-ranged interactions of nanoparticles with soft networks, such as synthetic gels and biological tissues. In this paper, calculations are undertaken that identify a generalized Hückel limit for nanoparticles in low-conductivity gels, and a new Smoluchowski limit for polyelectrolyte-coated particles in high-conductivity gels that is independent of the gel permeability. Also of fundamental interest is a finite, albeit small, electrophoretic mobility for uncharged particles in charged gels. Electrophoretic mobilities and drag coefficients (with electroviscous effects) for nanoparticles bearing non-uniform coronas show that relaxation effects are typically weak for the small nanoparticles (radius ≈ 3–10 nm) to which gel-electrophoresis has customarily been applied, but are profound for the larger nanoparticles (radius $\gtrsim 40$ nm in low conductivity gels) to which passivated gel-electrophoresis experiments have recently been applied. To demonstrate its practical application, the model is applied to (pH charge regulating) carboxylated polystyrene nanospheres in low-density passivated agarose gels (weak steric effects). This furnishes a new theoretical interpretation of literature data for which a finite diffuse-layer-thickness, pH-charge regulation, high charge, and relaxation effects dominate over the steric influences.

1 Introduction

Nanoparticle gel-electrophoresis has been applied in the last decade to sort many kinds of nanoparticles[9,10,23,27,28]. Experiments are conducted by depositing nanoparticle dispersions into the wells of a hydrogel slab (often agarose for nanoparticle gel-electrophoresis) to which a longitudinal electric field is applied. Nanoparticles migrate into the gel, and acquire an average translational velocity that generally reflects a complex coupling of electrical, hydrodynamic (long-range), and steric (short-range) interaction forces.

Gels are selected to adjust the balance of long- and short-range forces and, thus, optimize separation efficiency. In the limit where the particles are small compared to the gel pores (and the particles do not adhere to the gel), the gel serves to eliminate macroscale advection, thus enabling separations that reflect the free-solution electrophoretic mobility, which varies with nanoparticle architecture, e.g., size and charge, as imparted by a core and/or macromolelcular coatings[9,10]. However, in gels where the pore and particles sizes are comparable (again in the absence of adhesive interactions), hydrodynamic interaction hinders the mobility according to particle size.

Decreasing the pore size strengthens interaction with the gel so that particle dynamics may become intimately coupled to spatial and temporal fluctuations in the pore network. For example, Zhu and Mason[27] quantified how varying the mesh size of passivated agarose gels arrests electrophoretic migration above a threshold gel concentration that varies systematically with the particle size. Similar steric arrest has been gleaned from the the dynamic mobility (measured at MHz frequencies using electroacoustic spectroscopy) of silica nanoparticles in agarose gels[1].

[a] Department of Chemical Engineering, McGill University, 3610 University Street, Montreal, Quebec, H3A 0C5, Canada. Fax: +1 514 398 6897; Tel: +1 514 398 6678; E-mail: reghan.hill@mcgill.ca

Initiatives have been taken to minimize or completely eliminate steric the influences. This can been achieved by systematically changing the gel concentration, and using Ferguson analysis to extrapolate mobilities to zero gel concentration, thus expediting quantitative interpretation of the data using theory for free-solution electrophoresis[23], i.e., without steric or hydrodynamic interaction. However, systematically varying the gel concentration is time intensive, and may not be feasible for samples that are expensive or available in limited quantities. Thus, theories have been developed to model the long-range interactions, which tend to hinder electrophoretic migration[3,9]. Another approach is to passivate gels by incorporating uncharged polymers or surfactants according to the specific nanoparticle surface chemistry. Passivated agarose gels have expedited nanoparticle separations on the basis of size[27] and surface charge[28].

This paper addresses the electrokinetic and hydrodynamic factors that contribute to the more general nanoparticle gel-electrophoresis problem, using a continuum framework that adopts the Brinkman model for the hydrodynamic interaction. A comprehensive theory that unites electrokinetic and steric influences in a theoretically meaningful and practically useful manner is presently unavailable, and is likely to remain so for some time.

Steric influences have been studied in the literature on solute-diffusion in hydrogels, e.g., as reviewed by Amsden[4]. One such model, which accounts for the gel concentration and segment size and shape, was integrated into the gel-electrophoresis electrokinetic model of Allison et al.[3] In the more recent work of Allison et al.[2], this manifests as a force that adds to the hydrodynamic drag (proportional to the mean translational velocity). When this force is expressed as a ratio of the hydrodynamic drag, $\gamma \ll 1$, the electrophoretic mobility without steric friction can be conveniently multiplied by a steric factor $1/(1+\gamma) \approx 1-\gamma < 1$. Doane et al.[9] proposed a friction model for PEGylated gold nanoparticles that attempts to capture friction between PEG chains and an agarose skeleton due to dynamic entanglement. For polystyrene nanospheres in agarose gels, Zhu and Mason[27] recently proposed a thermally-driven hopping model to describe the time-average translation manifesting from the electrical force and fluctuating voids. Interestingly, this describes experimentally observed transitions from a mean velocity that is linear in the electric-field strength at low field strengths to one that becomes highly non-linear at high field strengths, albeit with a mechanical compliance factor that changes sign with the particle size. However, high electric-field strengths also manifest in non-linear electrokinetics[7], and it is presently unknown when and how to distinguish these. Yet another body of work has addressed the electric-field-induced dynamics of particles that are permanently adhered to or entrapped in hydrogel networks[1,18,26]; these studies complement an extensive microrheology literature[25].

To close the gap between gel-electrophoresis models (reviewed below), which are presently fragmented, and more advanced models for free-solution electrophoresis, this paper unites bare-particle gel-electrophoresis and free-solution electrophoresis models, accommodating charge-regulating coronas and gels, multi-component electrolytes, non-linear electrostatics, and polarization and relaxation effects*. These attributes tremendously simplify the interpretation of experiments with weak steric forces, because the overall model has a well-defined and complete set of parameters, and is not subject to untested simplifying assumptions. Such a model may expedite experiments using low-conductivity gels in which the signal-to-noise ratio can be maximized, and Joule heating and particle aggregation minimized.

The first nanoparticle gel-electrophoresis electrokinetic model was developed by Allison et al.[3] for bare spherical particles in uncharged gels, accounting for non-linear electrostatics and relaxation effects. As highlighted above, this model also accounted for steric friction. The theory was motivated by experiments[23] in which the hydrogel was assumed to bear zero charge, thus enabling the ion and charge distributions around a nanoparticle to be approximated by those that prevail in an electrolyte without gel. Moreover, when subjected to an electric field, electroosmotic flow (also termed electroendoosmotic flow) in the gel is driven only by the nanoparticle counter charge. As amply demonstrated by the challenges in solving similar equations for free-solution electrophoresis[15,19,20], the mathematical solution of the model equations was obtained via a numerical method having a rigorous analytical foundation.

More recent experiments of Doane et al.[9] with polymer-coated gold nanoparticles furnished evidence of agarose gels bearing a net negative charge, as evidenced by an uncharged molecular tracer (vitamin B12) attaining a finite positive electrophoretic mobility. Despite the nanoparticles bearing a negative charge (on the gold surface), positive electrophoretic mobilities where registered with high-molecular weight uncharged grafted polymer (PEG) coronas. Doane et al.[9] developed an analytical-approximate theory to model how charge on the gel (and its counter charge in the electrolyte) controls the nanoparticle mobility. This theory did not explicitly model the PEG coronas, but approximated the soft particles using a bare-sphere model with a modified surface potential. Since the relatively thick, uncharged coronas significantly reduce the apparent surface potential, the electrostatics were treated in the linear Debye-Hückel approximation under conditions where the Debye length is large compared to the nanoparticle radius. This theory also modelled a steric friction between the particle and gel, furnishing a gel-concentration dependent electrophoretic mobility that captured a mobility reversal with respect to the PEG molecular weight.

Subsequent theoretical studies removed restrictions on the relative magnitudes of the Debye length and particle size, also explicitly accounting for soft (albeit perfectly uniform) coronas[17]. These furnished a strong foundation for testing more intricate computations that account for non-linear electrostatics and relaxation effects. For example, Bhattacharyya et al.[7] adopted a direct discretization methodology (finite-volume) to capture the

* "Polarization and relaxation" is customarily used to identify the consequences of ion-electromigration and diffusion causing the ion-concentrations to deviate from their equilibrium values. Such perturbations cause the free-charge density to deviate from its equilibrium value, thereby perturbing the equilibrium electrostatic potential, e.g., modifying the induced electrostatic dipole moment. This perturbs the forces acting on a particle, generally decreasing its electrophoretic mobility.

polarization and relaxation effects for bare particles in uncharged gels, also addressing non-linear effects arising from strong electric fields. A very similar study, using the same direct-solution methodology, was undertaken by Bhattacharyya and De [6] for charged gels and strong electric fields.

While the foregoing direct-solution methodologies have the obvious benefit of furnishing solutions without simplifying the governing equations (e.g., based on symmetry and linearity considerations), the computational cost may be unnecessarily high for applications where the applied electric field is weak. Such computations are also unnecessarily expensive for parametric studies and fitting model parameters to experimental data, although they will be essential for experiments in which the electric-field strengths are particularly high (possibly requiring external cooling to eliminate Joule heating). Direct-solution methods have been critiqued for imprecise application of far-field boundary conditions (i.e., forcing the disturbances to zero at a finite radial position). Allison et al. [2] noted that direct solutions of the electrokinetic equations for gel-electrophoresis in the literature have furnished erroneous results.

Using methods developed specifically for free-solution electrophoresis, Hill [11] examined the non-linear electrostatics and relaxation effects for bare spheres in charge regulating gels, i.e., gels in which the charge on the skeleton is coupled to the local electrolyte ion concentrations. In this model, particular attention was given to the electrolyte composition and identity of the hydrogel counterions. Hill considered primary and secondary ion- and charge-density perturbations, showing that the primary perturbations (furnished by the equilibrium state) are the most important. The dominant counterion, which can change with the addition of salt (e.g., NaCl) to a gel that has H^+ counterions, for example, was demonstrated to profoundly influence the electroviscous and relaxation effects. Moreover, the electrophoretic mobility in the reference frame that translates with the bulk electroosmotic flow in the gel (hereafter termed the relative electrophoretic mobility) is practically independent of the gel charge. Hill also identified the relative electrophoretic mobility as being very closely related to the free-solution mobility, as furnished by the well-known theory of O'Brien and White [19], but reduced according to the hydrodynamic interaction with the gel. For bare particles in gels, the hydrodynamic hinderance factor is furnished by Brinkman's theory [8], depending only on the ratio of the particle radius to the square-root of the hydrogel permeability.

Most recently, Allison et al. [2] addressed non-linear electrostatics and the relaxation effects for spheres bearing uniform coatings in charged gels; this, in some sense, completed the general electrokinetic problem pioneered by Allison et al. [3] for bare particles in uncharged gels. Similarly to bare particles, the electrophoretic mobility of polyelectrolyte-coated particles in the reference frame that translates with the bulk electroosmotic flow in a gel was found to be practically independent of the gel charge. Allison et al. also identified strong relaxation effects at intermediate ionic strengths when the electrostatic potential on the particle surface is fixed. By varying the hydrogel permeability, it can be seen that the relative electrophoretic mobility in a gel is closely related to its free-solution mobility.

Many of the soft polymeric coronas used to sterically stabilize or functionalize nanoparticles are far from being uniformly permeable or uniformly charged. Thus, theoretical interpretations of the free-solution electrophoretic mobility of soft nanoparticles have benefitted from models of the corona architecture [11,14]. Nanoparticle coronas reflect the polymer attachment mechanism (e.g., physical adsorption versus terminal grafting), surface curvature (nanoparticle radius is generally comparable to ligand size), and a non-uniform distribution of ligand charge (e.g., PEG ligands bearing charged end groups [10]). Thus, while intricate models for free-solution electrophoresis have reached a relatively advanced state, it is unknown how the mobility is affected when particles are transferred to a gel.

This rest of this paper is organized as follows. After setting out the theory in section 2, its is validated, in part, by direct comparisons with analytical theory and independent computations (sections 3.1–3.2). Section 3.1 addresses the mobility of uncharged bare spheres in charged gels, highlighting that a small but finite mobility reflects the particle dielectric constant, even when polarization effects are accounted for. This section also provides a direct validation of an analytical theory that captures relaxation effects. Section 3.2 provides direct comparisons with independent calculations of Allison et al. [2] for particles with uniform (step-like) coatings. The low-ionic-strength (Hückel) limit in which the electrophoretic mobility and diffusion coefficient furnish the net particle charge is revealed. Also identified is a high-ionic-strength limit for polyelectrolyte-coated spheres in which the mobility is independent of the gel permeability. The model is applied in section 3.3 to study how corona architecture affects the electrophoretic mobility and the degree to which a perfectly uniform coating might approximate more realistic inhomogeneous coatings. Section 3.4 applies the model to gold nanoparticles bearing inhomogeneous (PEGylated) coronas bearing peripheral charge. Highlighted is how the polarization and relaxation effects depend on nanoparticle size and charge. Interestingly, polarization and relaxation are found to reflect the charge, which scales with the square of the particle size. Thus, small nanoparticles exhibit weak polarization and relaxation effects, whereas larger nanoparticles exhibit profound relaxation effects. Finally, section 3.5 interprets experiments of Zhu and Mason [28] to separate carboxylated polystyrene nanoparticles using passivated gels. These calculations demonstrate surface-charge regulating aspects of the more general electrokinetic model. Quantitative interpretations of the experiments are proposed, and several recommendations are suggested for reporting and interpreting gel-electrophoretic mobilities. Conclusions are summarized in section 4.

2 Theory

The fundamental equations, applied outside the particle core with radius a, surface charge density σ, and dielectric constant $\varepsilon_0\varepsilon_p$, comprise the Poisson, ion-conservation, and fluid momentum and mass conservation equations. These are well known, and, in the notation of Hill [11], are

$$-\varepsilon_0\varepsilon_s\nabla^2\psi = \rho_m + \rho_f,$$

$$0 = -\vec{\nabla}\cdot\left(n_i\vec{u} - D_i\vec{\nabla}n_i - z_i e\frac{D_i}{k_BT}n_i\vec{\nabla}\psi\right) \quad (i=1,...,N),$$

$$0 = \eta\nabla^2\vec{u} - \vec{\nabla}p - \frac{\eta}{\ell_c^2}(\vec{u}-\vec{V}) - \frac{\eta}{\ell_g^2}\vec{u} - \rho_m\vec{\nabla}\psi,$$

$$\vec{\nabla}\cdot\vec{u} = 0$$

with

$$\rho_m = \sum_{j=1}^{N} z_j e n_j \text{ and } \rho_f = \sum_{j=1}^{N}\rho_{f,j}.$$

Here, ψ is the electrostatic potential, $\vec{u}$ and p are the fluid velocity and pressure, and n_j are the mobile-ion concentrations with each ion having its distinct charge $z_j e$ and mobility $D_j/(k_BT)$, where D_j is a diffusion coefficient, k_BT is the thermal energy, and e is the fundamental charge. Furthermore, ρ_m and ρ_f denote the mobile (in the electrolyte) and immobile (on the corona and gel skeletons) charge densities . Physical properties include the solvent/electrolyte dielectric constant $\varepsilon_0\varepsilon_s$ and shear viscosity η.

The Brinkman screening length for the corona or gel, $\ell_{c/g}$, is related to number densities of Stokes resistance centers $n_{s,c/g}$, which exert a drag force (per unit volume) on the fluid $-6\pi\eta F_s a_{s,c/g}(\vec{u}-\vec{u}_s)$, where $F_s a_{s,c/g}$ is the hydrodynamic radius of a center with physical radius $a_{s,c/g}$, $F_s \geq 1$ is a dimensionless function of the total resistance-center volume fraction $\phi = (n_{s,c}a_{s,c}^3 + n_{s,g}a_{s,g}^3)4\pi/3$, and $\vec{u}_s$ is the segment velocity. It follows that $\ell_{c/g}^{-2} = 6\pi F_s a_{s,c/g} n_{s,c/g}$. For segments that form the corona, $\vec{u}_s = \vec{V}$ (particle velocity); whereas $\vec{u}_s = 0$ for segments that form the (stationary) gel.

Solutions of the foregoing equations are sought when the particle and gel are subjected to a uniform electric field $\vec{E}$ in the absence of a far-field pressure gradient. Under these conditions, the particle attains a steady translational velocity $\vec{V}$, which, based on linearity and symmetry considerations, is co-linear with $\vec{E}$. Charge on the gel also drives an electroosmotic flow in the far field with fluid velocity [12]

$$\vec{U} = \vec{U}_{eo} \equiv \frac{\rho_m^0 \ell_g^2}{\eta}\vec{E},$$

where ρ_m^0 is the equilibrium mobile charge density in the gel (minus the equilibrium fixed-charge density ρ_f^0). To satisfy the model equations, boundary conditions, and the particle equation of motion, the equations are first solved at equilibrium ($\vec{E} = \vec{V} = \vec{U} = 0$), furnishing an equilibrium electrostatic potential ψ^0, mobile ionic concentrations n_j^0, and fixed charges $\rho_{f,j}^0$ (complimentary to each mobility-ion species). This requires solutions of a non-linear Poisson-Boltzmann equation, which are obtained using Newton iteration with an adaptive finite-difference grid. The equilibrium variables are then linearized about their equilibrium values and computed when the particle is translated at a velocity $\vec{V}$ (forcing vector $\vec{X} = \vec{V}$) or subjected to an electric field $\vec{E}$ (forcing vector $\vec{X} = \vec{E}$). The linearized equations for the so-called E- and V- problems are then superposed to satisfy the boundary conditions and particle equation of motion. Technical details, including those accounting for charge-regulation chemistry, are available elsewhere [14], and so only essential modifications to the earlier formulations are highlighted here.

In this paper, the model is applied with $N = 4$ electrolyte-ion species (indices $j = 1$, ..., 4) corresponding to H^+, Cl^-, Na^+ and OH^-. Unless stated otherwise, fixed charge on the corona and gel comes from the complete dissociation of H^+ (index $j = 1$). Thus, the equilibrium dissociation constants for the underlying charge-regulation models are generally set to values that eliminate charge regulation; under these conditions, it follows that the total fixed charge ρ_f (from the corona and gel) equals the equilibrium contribution from the dissociation of H^+, i.e., $\rho_f = \rho_{f,1}^0$.

The forces on the core-corona composite are from electrical and hydrodynamic tractions and body forces, obtained by adding those recently derived for soft spheres in Newtonian electrolytes [11] to those for bare spheres in gels [12] and subtracting the common terms, giving

$$\begin{aligned}
\vec{F}^X &= -(4/3)\pi a^2\vec{X}[\eta(\hat{f}_{rrr}a + \hat{f}_{rr} - 6\hat{f}_r a^{-1} + 6\hat{f}a^{-2}) - \rho_m^0(\hat{\psi} - aE/X)] \\
&- \sigma(4/3)\pi a^2\vec{X}[\hat{\psi}_r + 2\hat{\psi}a^{-1} - 3E/X] + (4/3)\pi a^3\vec{V}\eta\ell_g^{-2} \\
&+ (4/3)\pi\vec{X}\int_{r=a}^{\infty}\{\rho_f^0[3r^2E/X - (\hat{\psi}r^2)_r] - \sum_{j=1}^{N}\hat{\rho}_{f,j}r^2\psi_r^0\}\mathrm{d}r \\
&+ (4/3)\pi\eta\vec{X}\int_{r=a}^{\infty}\ell_c^{-2}[2(\hat{f}r^2)_r + 3r^2(U-V)/X]\mathrm{d}r. \qquad (1)
\end{aligned}$$

The hatted variables are radial functions furnishing the perturbations to the fluid velocity, $\vec{u}(\vec{r}) = \vec{\nabla}\times[f(r)\vec{X}\times\vec{e}_r] + \vec{U}$, electrostatic potential, $\psi(\vec{r}) = \psi^0(r) + \hat{\psi}(r)\vec{X}\cdot\vec{e}_r - \vec{E}\cdot\vec{r}$, electrolyte ion concentrations, $n_j(\vec{r}) = n_j^0(r) + \hat{n}_j(r)\vec{X}\cdot\vec{e}_r$, and fixed charge densities, $\rho_{f,j}(\vec{r}) = \rho_{f,j}^0(r) + \hat{\rho}_{f,j}(r)\vec{X}\cdot\vec{e}_r$ [11,12]. All the functions in Eqn. (1) not in the integrands of the two radial integrals are evaluated on the core surface (radial position $r = a$).

The (dimensional) absolute electrophoretic mobility†

$$M = V/E$$

is obtained by solving (i) a so-called V-problem in which the particle translates with velocity $\vec{V}$ in an electrolyte that is stationary in the far field ($\vec{U} = 0$) with no applied electric field ($\vec{E} = 0$), furnishing a force $\vec{F}^V = F^V\vec{V}$; and (ii) a so-called E-problem in which the particle is stationary ($\vec{V} = 0$) when subjected to an electric field $\vec{E}$, furnishing a force $\vec{F}^E = F^E\vec{E}$. In both problems, the far-field pressure gradient is taken to be zero. Then, applying the principle of linear superposition, the particle equation of motion $\vec{F}^V + \vec{F}^E = 0$ furnishes a mobility

$$\frac{V}{E} = -\frac{F^E}{F^V},$$

which is valid when the applied electric field is sufficiently weak.

A careful comparison of the foregoing equations and boundary conditions with those underlying the MPEK package, for example, reveals that they can be solved with modifications to the computer code that solves the soft-sphere electrokinetic model of Hill et al. [15]. In particular, these modifications entail: (i) introduction of separate Stokes-resistance-center and fixed-charge density profiles for the corona and gel phases; (ii) adding these contributions

† Note that variables V, E, U, U_{eo} are the signed magnitudes of the respective (co-linear) vectors; so, for example, $\vec{E} = E\vec{e}_z$, where $\vec{e}_z$ is a unit vector in the z-direction.

to the appropriate entries of the global matrix of finite-difference coefficients; (iii) changing the exponents for the far-field power-law decay of the fluid velocity to reflect Brinkmanlets (rather than Stokeslets); and (iv) evaluating the forces directly, using Eqn. (1), rather than via the asymptotic coefficients for the far-field decay of the fluid velocity. In both the foregoing V- and E-problems, the far-field velocity disturbances decay as r^{-3} (Brinkmanlet) rather than the more familiar r^{-1} (Stokeslet) as $r \to \infty$[13].

The computer code was thoroughly tested by making direct comparisons with: (i) analytical theory for uncharged spheres in gels, including relaxation effects; (ii) independent calculations from recent literature addressing core-shell particles with perfectly uniform coronas, without charge regulation; (iii) previously calculated mobilities and drag coefficients for bare spheres in gels, with and without charge regulation; and (iv) previously calculated free-solution mobilities and drag coefficients for core-shell particles bearing complex, charge regulating coronas. All the results presented below, with the exception of a theoretical interpretation of experiments reported by Zhu and Mason[28], neglect charge regulation.

3 Results and discussion

We will focus primarily on the particle velocity relative to the bulk electroosmotic flow, thus motivating the dimensionless relative/intrinsic electrophoretic mobility

$$M^* - M^*_{eo} = \frac{3\eta e}{2\varepsilon_s \varepsilon_0 k_B T} \frac{(V - U_{eo})}{E}.$$

In the next two subsections, the coronas have a Stokes-resistance-center density profile (three parameters $n_{s,c,0}$, L and δ)

$$n_{s,c}(r) = n_{s,c,0} 0.5 \mathrm{erfc}[-(r - L - a)/\delta], \tag{2}$$

as depicted in figure 1. Note that this becomes a step-like distribution (as adopted in the soft-sphere model of Allison et al.[2] and others) when $\delta/L \to 0$. For these coronas, the fixed charge density is taken to be proportional to $n_{s,c}(r)$, so (three parameters $n_{f,c,0}$, L and δ)

$$\rho_{f,c}(r) = -e n_{f,c,0} 0.5 \mathrm{erfc}[-(r - L - a)/\delta]. \tag{3}$$

A more sophisticated Stokes-resitance-center and fixed-charge density profiles are adopted below to model nanopaticles bearing uncharged ligands with charged end-groups, otherwise termed peripheral charge[14].

While the fixed charge densities in this paper mostly correspond to the complete dissociation of H^+, the computer program developed permits the user to prescribe, for all of the N ion species (indices $j = 1, ..., N$), a radial number density $n_{s,c/g,j}(r)$ of Stokes resistance centers, each having Stokes radius $a_{s,c/g,j}$, and a radial number density of binding sites $n^*_{f,c/g,j}(r)$ with valence $-z_j$, and equilibrium dissociation constants (two for each species) $K_{1/2,c/g,j}$.

For simplicity, the gels are prescribed to be uniform, so $n_{s,g}$ and $\rho_{f,g}$ are constants, and all the equilibrium dissociation constants are set so that there is either zero or complete dissociation of H^+, and zero dissociation or association of all other ions from the corona and gel. It follows that the total Stokes-resistance-center and fixed-charge densities are $n_s(r) = n_{s,c}(r) + n_{s,g}$ and $\rho_f(r) = \rho_{f,c}(r) + \rho_{f,g}$ with $r \geq a$.

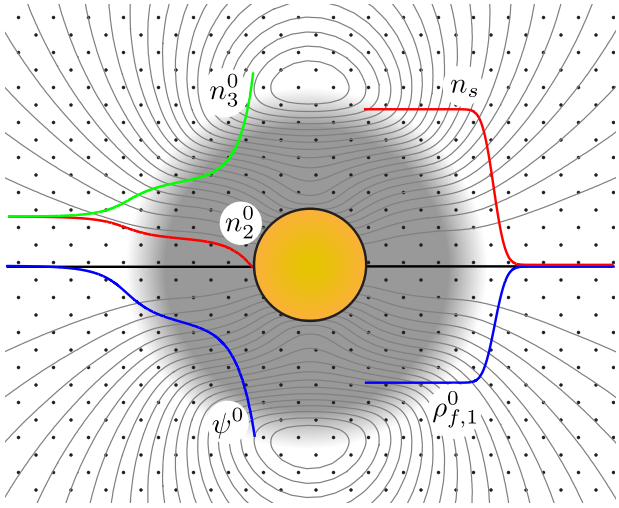

Fig. 1 Schematic of a charged polyelectrolyte-coated nanoparticle undergoing electrophoresis in a charged hydrogel (with prototypical core-shell architecture) according to Eqns. (2) and (3). Here, negative charge is immobilized on the core surface (surface charge density σ) and throughout the corona and gel (fixed charge density $\rho_f = \rho^0_{f,1}$ from the dissociation of H^+) with the corona segment density n_s predominantly uniform within a distance L of the core surface. Moreover, fixed charge comes from the dissociation of H^+ with the dominant ions (here at high bulk ionic strength) within the corona being Na^+ (equilibrium concentration n^0_3) and Cl^- (equilibrium concentration n^0_2). Streamlines depict fluid motion (on the symmetry plane) during force-free electrophoretic translation, co-linear with a horizontal applied electric field.

The model and its numerical solution are complex, motivating a thorough testing of the newly developed computer code by direct comparison to independent analytical and numerical solutions, albeit in limited regions of the parameter space. The next two subsections undertake such tests, also uncovering new physical and mathematical insights into the more general gel-electrophoresis problem; these include a finite mobility for uncharged dielectric spheres in charged gels, Hückel and Smoluchowski limits for soft spheres in gels, and a quantitative interpretation of passivated gel-electrophoresis data for charge-regulated nanospheres (with weak steric interaction).

3.1 Uncharged dielectric spheres in charged gels

An interesting test case, for which an exact analytical formula is available to capture relaxation effects, is the electrophoretic translation of an uncharged sphere in a charged gel. Mohammadi and Hill[18] derived an exact analytical formula for the electric-field-induced force on such a sphere (radius a_h) *immobilized* in a charged, compressible gel (charge density ρ_f and permeability ℓ^2). For the incompressible gels of interest here, the electric-field-induced force is

$$\vec{F}^E_{MH} = -6\pi a \ell^2 \rho_f [1 + a/\ell + (a/\ell)^2/3]\vec{E} + \frac{2\pi a^3 \rho_f [(\kappa a + 1)^2 + 1]\vec{E}}{(\kappa a + 1)^2 + 1 + (\varepsilon_p/\varepsilon_s)(\kappa a + 1)},$$

which becomes independent of the ionic strength when the dielectric contrast between the particle and electrolyte is very large, and otherwise varies with the ionic strength because of relaxation effects. Whereas the free-solution electrophoretic mobility of bare spheres is independent of the particle dielectric constant when the relaxation effects are accounted for[19], the theory of Mohammadi and Hill shows that the electrical force in charged gels actually depends on the dielectric contrast. This interesting result seems to have been overlooked in the literature, and the theory has yet to be verified by an independent numerical calculation.

To make such a comparison, note that drag force on an uncharged sphere translating in a gel is[13,22]

$$\vec{F}_B^V = -6\pi\eta a F_B(a/\ell)\vec{V},$$

where the Brinkman factor

$$F_B(a/\ell) = 1 + a/\ell + (a/\ell)^2/9. \tag{4}$$

Thus, from the particle equation of motion, $\vec{F}_{MH}^E + \vec{F}_B^V = 0$, a (dimensional) absolute electrophoretic mobility is predicted:

$$M = -\frac{\rho_f \ell^2}{\eta}\left\{\frac{1 + a/\ell + (a/\ell)^2/3 - \frac{(1/3)(a/\ell)^2[(\kappa a+1)^2+1]}{(\kappa a+1)^2+1+(\varepsilon_p/\varepsilon_s)(\kappa a+1)}}{1 + a/\ell + (a/\ell)^2/9}\right\}. \tag{5}$$

The relative mobility, which is small but finite, is shown in figure 2 with particle dielectric constants $\varepsilon_p = \varepsilon_s/2$ (a) and $2\varepsilon_s$ (b). These furnish mobilities that vary with the ionic strength because of relaxation effects. There is clearly excellent agreement between the numerical and analytical solutions at all ionic strengths, thereby (i) independently validating the analytical theory of Mohammadi and Hill[18] and (ii) verifying, in part, the present numerical solution. Calculations undertaken with $\varepsilon_p/\varepsilon_s \to 0$ and $\varepsilon_p/\varepsilon_s \to \infty$ (not shown) were indeed independent of the ionic strength, as predicted by Eqn. (5), attaining negative (positive) relative mobilities when $\varepsilon_p/\varepsilon_s \to 0$ (∞). In figure 2, the numerical calculations undertaken without the ion-concentration perturbations (dashed lines) are independent of the ionic strength; these also show that the relaxation effects vanish at low ionic strength ($\kappa a \to 0$). Interestingly, the calculations with and without relaxation effects asymptote to distinctly different limits at high ionic strength, agreeing only at vanishing ionic strength.

3.2 Step-like coronas

Rarely addressed is that the mobility should asymptote the analogue of the well-known Hückel mobility for free-solution electrophoresis of bare particles (when neglecting steric friction in gels) at vanishing ionic strength. This limit holds irrespective of the particle charge, and is generally difficult to resolve numerically, because the Debye length must be very large compared to the particle radius. Under these conditions, an extremely high electrostatic potential (at fixed particle charge) may prevail, necessitating solutions of the non-linear Poisson-Boltzmann equation. Such challenges were highlighted by Allison et al.[2], who noted that their computational method is limited to κa varying over a several decades centred on $\kappa a \sim 1$. As demonstrated below, the

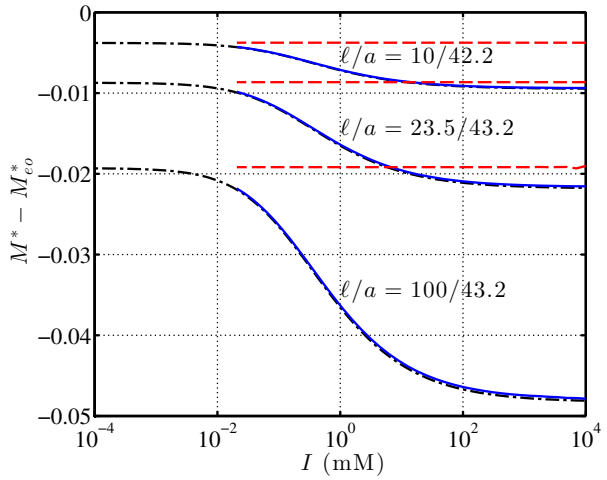

(a) $\epsilon_p = \epsilon_s/2$

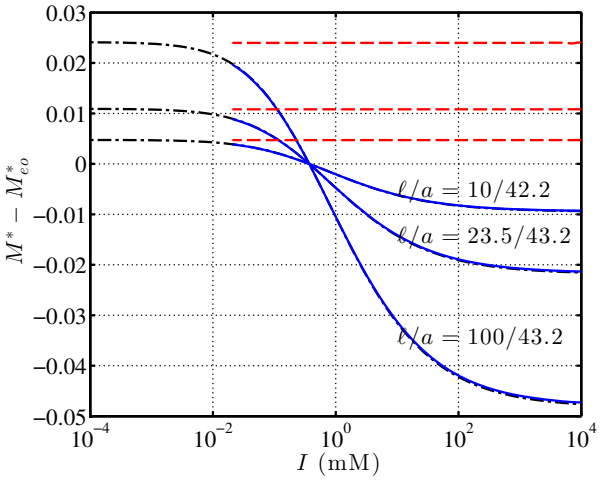

(b) $\epsilon_p = 2\epsilon_s$

Fig. 2 Gel-electrophoretic mobilities for uncharged bare spheres (a = 43.2 nm) with dielectric constant $\varepsilon_p = \varepsilon_s/2$ (a) and $2\varepsilon_s$ (b) in charged gels ($\rho_f = -4$ kC m^{-3}): $\ell = 10$, 23.5 and 100 nm (top to bottom). Solid (dashed) lines are numerical calculations with (without) the relaxation effects, and dashed-dotted lines are from Eqn. (5).

Hückel limit is generally not realized for nanoparticles with the (small) size and charge considered by Allison et al. until $\kappa a \lesssim 10^{-2}$. Moreover, we will see that for larger and more highly charged nanoparticles, the Hückel limit is realized only when $\kappa a \lesssim 10^{-4}$.

In the Hückel limit, the bare Coulomb force $ze\vec{E}$ balances the hydrodynamic drag $-6\pi\eta a_h(\vec{V} - \vec{U}_{eo})$ (both irrespective of the nanoparticle architecture), furnishing a (dimensional) relative electrophoretic mobility‡

$$M - M_{eo} = \frac{ze}{6\pi\eta a_h} \quad (\kappa a \to 0), \tag{6}$$

‡ The symbol $M_{eo} = U_{eo}/E$ denotes an electroosmotic mobility for the gel, so $M - M_{eo} = (V - U_{eo})/E$ is the particle's relative electrophoretic mobility, i.e., the mobility in a frame of reference translating with velocity U_{eo}.

where $a_h/a = F(L/a, \ell_c/a, \ell_g/a) \geq 1$ is the ratio of the effective hydrodynamic radius a_h to the core radius a. Note that a_h depends on the corona thickness L, corona Brinkman length ℓ_c, and medium/gel Brinkman length ℓ_g [13]. In this study, the net particle valence (arising from charge on the core and corona) is conveniently ascertained by numerically evaluating the integral [16]

$$z = \sum_{j=1}^{N} n_j^{\infty} z_j \int_a^{\infty} (e^{-z_j e\psi^0/(k_B T)} - 1) 4\pi r^2 \mathrm{d}r. \qquad (7)$$

The resulting mobilities furnished by Eqn. (6) are shown in the figures below as horizontal dashed lines at low ionic strength. When compared to the full calculations, for which the smallest values of κa are limited by the solubility product of water to ionic strengths $\geq 10^{-4}$ mM, these provide compelling asymptotic limits that also validate, in part, the full calculations.

The mobility ionic-strength relationship for nanoparticles with charged cores, bearing various fixed surface charges and uncharged coronas, is shown in figure 3. With a few minor exceptions (set out in the figure caption), the parameters are the same as prescribed by Allison et al. [2] in their figure 4. Here, however, their calculations have been extended (from $\kappa a \sim 0.1$) to much lower ionic strengths where the foregoing Hückel limits are reached: abscissa $2 + \log_{10}(\kappa a) \lesssim 1$ for the most weakly charged particle (valence $z \sim -10$); and $2 + \log_{10}(\kappa a) \lesssim 0$ for the most highly charged particle (valence ~ -40). Thus, whereas Allison et al. noted that their theories with and without the relaxation effects converge to the same values at high ionic strengths, we now see that these also converge to the same values at vanishing ionic strength.

Calculations undertaken with (solid) and without (dashed) the relaxation effects show that these are significant only for the most highly charged particles at intermediate ionic strengths ($2 + \log_{10}(\kappa a) \sim 0.5$–$2$). At the higher ionic strengths for which mobilities were reported by Allison et al. [2], the independent solutions are readily verified to be in almost perfect agreement. There is one ostensible discrepancy between the mobilities for the highest charged particle (valence $z \approx -40$) without the relaxation effects at low ionic strengths.

A clue as to the source of the foregoing discrepancy comes from the limiting mobilities at vanishing ionic strength, reported by Allison et al. [2] to be ≈ -0.91, -1.86, and -3.73 for the particles with valences $z = -9.8$, -19.6, and 39.2, respectively. In figure 3, the limiting mobilities (horizontal lines) were independently calculated from Eqn. (6) using the valences prescribed by Allison et al. and the hydrodynamic size for these core-shell nanoparticles in the gel furnished by the exact theory of Hill and Li [13], $F = a_h/a \approx 1.694$. The resulting mobilities are ≈ -0.915, -1.83, and -3.66, whereas the limiting values from the full calculations, at the lowest ionic strength available (10^{-4} mM), are ≈ -0.913, -1.83, and -3.65 (with relaxation effects, and therefore with smaller mobility magnitude than without relaxation effects), and ≈ -0.913, -1.83, and -3.65 (without relaxation effects).

As to be expected, the full calculations undertaken here without the relaxation effects all fall slightly short of the exact limiting values, since the full calculations approach the limits with an increasing mobility magnitude. In contrast, the limits of Allison et al. [2], also without relaxation effects, have magnitudes that slightly *exceed* the exact values. Thus, while these discrepancies have negligible practical significance, they do identify subtleties that need to be resolved, presumably for highly-charged particles without the relaxation effects. These may reflect the low-charge approximation that Allison et al. [2] used to compute mobilities at the lowest ionic strengths[§].

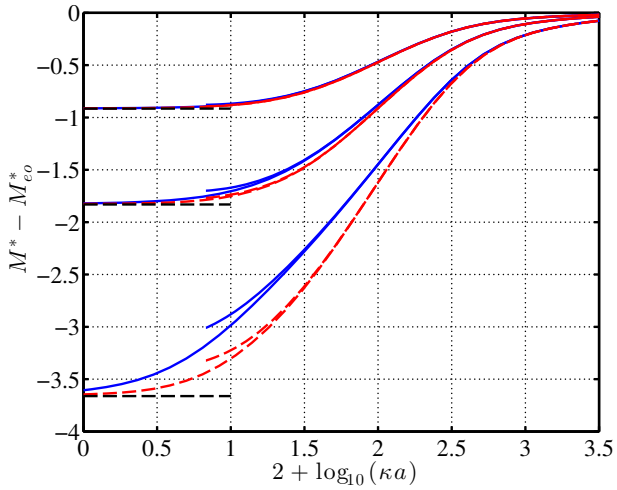

Fig. 3 Gel-electrophoretic mobilities for spheres ($a = 4.05$ nm) bearing different surface charge densities (valences $z = -9.8, -19.6, 39.2$) and a uniform uncharged coating ($L = 2$ nm, $\ell = 1$ nm). Particles are dispersed in uncharged ($\rho_f = 0$, $\ell = 14.33$ nm) and charged gels ($\rho_f = -5$ kC m^{-3}, $\ell = 14.33$ nm): the lower limit on κa (abscissa ≈ 0.75) identifies charged gels with vanishing added salt. Parameters are as prescribed in figure 4 of Allison et al. [2], except: (i) perfectly uniform (step) coatings are approximated here using a complementary error function (with $\delta/L = 1/100$); and (ii) the electrolyte here contains H^+ counterions of the charged gel with added NaCl and OH^- with $[H^+][OH^-] = 10^{-14}$ M^2. Red dashed lines are calculations without ion-concentration perturbation ("relaxation") terms. Horizontal lines are the Hückel mobility furnished by Eqn. (6). All mobilities (calculated without steric friction) have been multiplied by the steric factor $1/(1 + 0.1139)$ prescribed by Allison et al. [2]

A more challenging test is to calculate the mobilities of nanoparticles with a fixed core surface potential at high ionic strengths. In this limit, the Debye length becomes very small compared to the particle as the particle charge increases with increasing ionic strength. Despite a divergence of the charge with increasing ionic strength, the mobility remains finite, because the electrical force is balanced by a viscous shear force. Such calculations were demonstrated by Allison et al. [2] in their figure 7, again for very small nanoparticles bearing uncharged coronas. These data are reproduced in figure 4 using the present model. Again, it is readily verified that the independent computational methods (with relaxation effects) are in excellent agreement. At high ionic strengths

§ Mobilities calculated without the relaxation terms depend on the core dielectric constant. Here and elsewhere in this paper, the dielectric constant for the core $\varepsilon_p \ll \varepsilon_s$ when excluding the relaxation terms; this generates an electric-field-perturbation that drives electromigration fluxes that are tangent to the core surface, thus avoiding the requirement for normal diffusion fluxes (and therefore ion-concentration perturbations) to maintain a constant surface charge (and zero ion fluxes) at $r = a$.

$(2+\log_{10}(\kappa a) \gtrsim 4)$, both solution methods breakdown before the high κa asymptotes (analogues of the Smoluchowski limit for bare spheres) can be reached. For such small particles, however, the ionic strengths and accompanying surface charge densities (with fixed surface potentials) become so high as to be grossly unphysical.

A final point to be made from figure 4 concerns the relaxation effects, which are evidently very significant. However, a fixed particle charge (as applied in figure 3) generally furnishes a much more physically acceptable approximation, in which case relaxation effects impacting the interpretation of experiments with very small nanoparticles are much less significant than suggested by plots such as figure 4. This is because increasing the ionic strength while maintaining a fixed charge is accompanied by a decreasing electrostatic potential, placing all calculations in a regime where non-linear electrostatics and ion-concentration perturbations eventually become negligible. The relaxation effects for larger and, thus, generally more highly charged particles, are much more important, as discussed in the sections below.

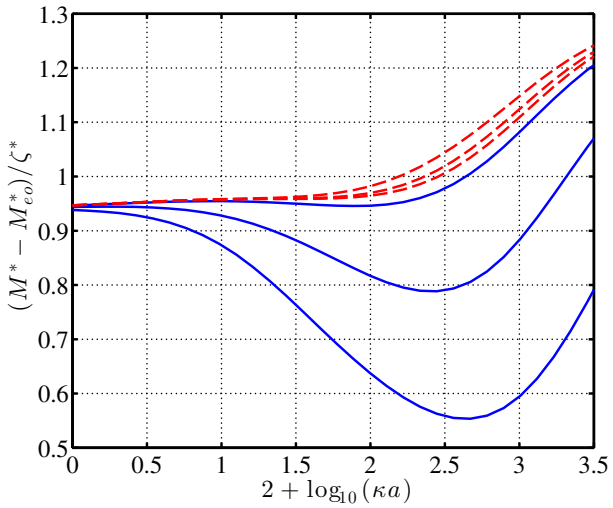

Fig. 4 Model and computational validation by reproduction of figure 7 of Allison et al.[2] for spheres ($a = 1$ nm) bearing different surface ζ-potentials ($\zeta^* = -1, -3, -5$) and a uniform, uncharged coating ($L = 0.5$ nm, $\ell = 1$ nm). Here, particles are dispersed in uncharged gels ($\rho_f = 0$, $\ell = 38.38$ nm). Dashed lines are calculations without ion-concentration perturbation ("relaxation") terms. Parameters are the same as Allison et al.[2], except: (i) their perfectly uniform (step) coatings are approximated here using a complementary error function (with $\delta/L = 1/100$); and (ii) the electrolyte here contains H^+ counterions of the charged gel with added NaCl and OH^- with $[H^+][OH^-] = 10^{-14}$ M^2. All mobilities (calculated without steric friction) have been multiplied by the steric factor $1/(1+0.0042)$ prescribed by Allison et al.[2]

3.3 Polyelectrolyte coronas

Having now verified the computational methodology, in part, by comparing results for core-shell nanoparticles having perfectly uniform coronas with previous literature, we turn to the gel-electrophoretic mobilities of nanoparticles with more complex and, therefore, more realistic coronas. For the polyelectrolyte-coated particles in this section, we will consider, in addition to the Hückel limit at low ionic strength, the limiting mobility at high ionic strength. Based on the well-known free-solution mobility for polyelectrolyte-coated particles at high ionic strength[15,20], the limiting (dimensional) relative mobility in a gel is found to be

$$M - M_{eo} = \frac{\rho_{f,c}\ell_c^2}{\eta} \quad (\kappa a \to \infty, \ell_c/L \ll 1, \ell_c/\ell_g \ll 1). \tag{8}$$

The gel permeability does not explicitly enter this formula, because the gel attenuates the external flows in the so-called V- and E-problems in exactly the same way. In the V-problem, the disturbance is that in a Brinkman medium with velocity $\vec{V}$ at the hydrodynamic radius a_h. In the E-problem, the electroosmotic flow disturbance generated by the particle at high ionic strength is one where the velocity at the hydrodynamic radius is the electroosmotic flow velocity $\vec{U}_{eo} = -\rho_{f,c}\ell_c^2\vec{E}/\eta$. Since the net forces on the particle in both problems arise from the external hydrodynamic disturbances (Brinkman flows), which only differ by the velocity at the particle surface, the particle equation of motion may be written without having to prescribe the gel-permeability-dependent prefactors, i.e., $-V + \rho_{f,c}\ell_c^2 E/\eta = 0$, which is Eqn. (8).

In this section, we also evaluate an hypothesis of Hill[12] that permits the gel-electrophoretic mobility for any nanoparticle architecture to be predicted from knowledge of its free-solution mobility and its diffusion coefficient in a gel. This approximation can be written

$$M - M_{eo} \approx \frac{M(\ell_g/a_h \gg 1)}{F_B(\ell_g/a_h)} \quad (\kappa a \ll 1, \ell_g/a_h \gtrsim 1), \tag{9}$$

where $M(\ell_g/a_h \gg 1)$ is the free-solution mobility, e.g., measured using a commercial light-scattering electrophoresis instrument or calculated theoretically with $\ell_g \gg a_h$, and F_B is the ratio of the drag coefficient (reciprocal Brownian diffusivity) in the gel to the drag coefficient in pure electrolyte.

The mobility of nanoparticles bearing uniformly charged coronas is shown in figure 5. Note that the coronas are not perfectly uniform, but have a diffuse periphery with $\delta = 0.1L$. For simplicity, they are fully charged, in the sense that the fixed charge density is proportional to the polymer segment density with no charge regulation. Six principal curves are shown for gels that are either highly permeable ($\ell_g = 100$ nm) or weakly permeable ($\ell_g = 10$ nm) with three charge densities $\rho^0_{f,g} = 0$, -1, -4 kC m^{-3}. The curves span the range of electrolyte ion concentrations from as low as 10^{-4} mM in uncharged gels containing pure water (and higher in charged gels with counterions) to 10 M (from added NaCl).

Approximations of the limiting mobilities at vanishing ionic strength are furnished by Eqn. (6) with $z \approx -68$ from Eqn. (7) and F_B from the theory of Hill and Li[13] for core-shell particles with perfectly uniform coronas. Since $\delta/L > 0$, F_B according to the theory of Hill and Li[13] is expected to be slightly higher than from the full calculation. Nevertheless, the approximation clearly provides a satisfactory extrapolation of the full calculations to vanishing ionic strength, highlighting that the differences in the mobilities reflect the different hydrodynamic drag coefficients in low- and high-permeability gels. At high ionic strength, the mobilities in the low- and high-permeability gels converge to the

value predicted by Eqn. (8), and are therefore independent of the gel charge and permeability, reflecting only the charge density and permeability of the nanoparticle corona. Finally, the three dashed curves in figure 5 are the mobilities in the low-permeability gel predicted using Eqn. (9), here using the relative mobilities from the high-permeability gels and F_B according to the theory of Hill and Li [13]. This clearly provides an increasingly accurate approximation with decreasing ionic strength, as predicted by Hill [12].

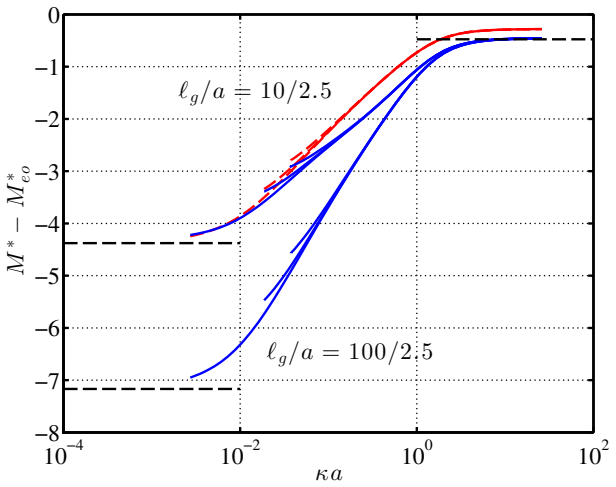

Fig. 5 Gel-electrophoretic mobilities of spheres ($a = 2.5$ nm, $\sigma = -1.5$ μC cm^{-2}) bearing uniformly charged coronas ($L = 5$ nm, $\delta = 0.5$ nm, $\ell_{c,0} = 1$ nm, $\rho^0_{f,c} = -n_s e/100$, $n_{s,0} \approx 5.87$ M, $a_s = 0.15$ Å) in gels with charge densities $\rho^0_{f,g} = 0, -1, -4$ kC m^{-3}, and $\ell_g = 10, 100$ nm. Dashed curves are mobilities in the low permeability gels ($\ell_g = 10$ nm) approximated using the mobilities in high-permeability gels ($\ell_g = 100$ nm) according to Eqn. (9) for $\kappa a \ll 1$. Horizontal lines are the low- and high-κa asymptotes according to Eqns. (6) and (8). The lower limit of κa for each curve identifies the ionic strength at vanishing added salt (10^{-7} M for uncharged gels containing pure water, and higher for charged gels containing pure water and counterions).

The approximate theories augmenting figure 5 were evaluated using the drag coefficient for core-shell particles (with perfectly uniform coronas) in gels. The exact drag coefficients, which account for the specific nanoparticle architecture, electroviscous effects, and the gel are provided in figure 6. The most significant influence is, of course, the hydrogel permeability. The electroviscous effects, which manifest as an ionic-strength dependent drag coefficient, vary with the hydrogel charge. For bare particles in gels, this has previously been attributed to the mobility of the dominant counterion. Here, the dominant counterion is the gel counterion H^+ when the added salt (NaCl) concentration is very low, and is otherwise Na^+. Because H^+ has an unusually high mobility, the electroviscous effects practically vanish as the concentration of Na^+ becomes small compared to that of H^+.

Figure 6 also shows the drag coefficient from the hydrodynamic theory (no electroviscous effects) of Hill and Li [13] for particles bearing perfectly uniform coronas. These furnish a lower bound on the exact drag coefficient, since (i) electroviscous effects are neglected, and (ii) the diffuse corona periphery (here $\delta = 0.1L$) increases its hydrodynamic thickness. Similarly to figure 5, the three dashed curves in figure 6 are obtained by multiplying the drag coefficient in the highly permeable gel by the ratio of the drag coefficient in the low-permeability gel to the value in the high-permeability gel, both approximated according to Hill and Li [13]. This shows that the electroviscous effects in the low-permeability gel are reasonably well captured by those in the high-permeability gel, and are therefore the same as in pure electrolyte (with the same dominant counterion).

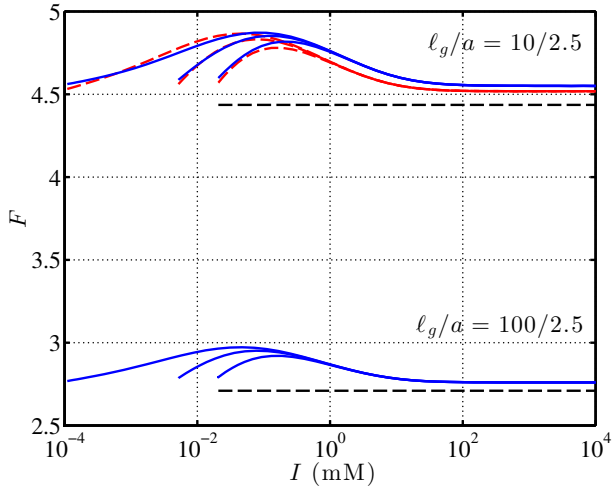

Fig. 6 Drag coefficients accompanying the mobilities in figure 5. Horizontal lines are for perfectly uniform, uncharged coronas ($\delta/L = 0$) according to Hill and Li [13].

The dimensionless electrostatic potential at the core surface is shown in figure 7. As expected, this increases in magnitude with decreasing ionic strength. With the prevailing (like signed) surface and corona charge densities, the transition from the Debye-Hückel region to the non-linear Poisson-Boltzmann domain, i.e., when $|\psi| \approx k_B T/e$ occurs when $I \sim 100$ mM. This corresponds to the growth of electroviscous effects in the drag coefficients (figure 6) and relaxation effects in the mobilities (figure 5). Charge on the gel (weakly) impacts the electrostatic potential to a similar degree as the relative mobilities.

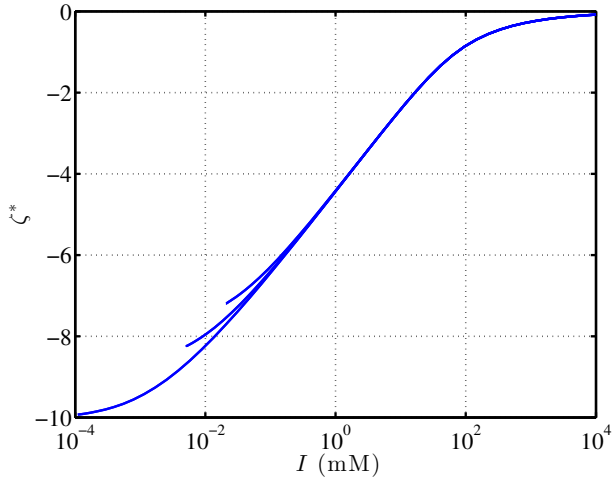

Fig. 7 Core surface potentials $\zeta^* = \zeta(r = a)e/(k_B T)$ accompanying the mobilities and drag coefficients in figures 5 and 6.

To gain a better understanding of the role that finer details of the corona segment density profile have on the relative mobilities and drag coefficient, figures 8 and 9 show how these quantities vary with the parameter δ that controls the rate at which the corona segment and charge densities decay from their nominal values ($n_{s,c,0}$ and $\rho_{f,c,0}$) to zero at the radial periphery $r-a \approx L$. Here, the relative mobility and drag coefficient are plotted versus δ/L at three concentrations of added NaCl, $I_s = 10^{-3}$, 1, and 10^3 mM (in uncharged gels).

Whereas the drag coefficients increase significantly with δ/L, in a manner that is practically independent of the ionic strength, the relative mobilities decrease with increasing δ/L, in manners that diminish with increasing ionic strength. Note that δ/L must be $\lesssim 0.1$ to reasonably approximate a perfectly uniform corona ($\delta/L = 0$). These calculations therefore elucidate the degree to which the results presented in figures 3 and 4, undertaken with $\delta/L = 10^{-2}$, compare with those of Allison et al.[2] ($\delta = 0$). There are no discernible difficulties in resolving a corona that has very rapid changes in segment and charge density. This is not surprising, perhaps, given that the methodology resolves large gradients in the fluid velocity, electrostatic potential, and ion concentrations when $\kappa a \gg 1$. Note that the exact drag coefficient agrees exactly with the hydrodynamic theory of Hill and Li[13] when (i) δ/L is sufficiently small ($\delta \ll 0.1L$) and (ii) the ionic strength is high enough to fully attenuate the electroviscous effects ($I_s \gg 1$ mM).

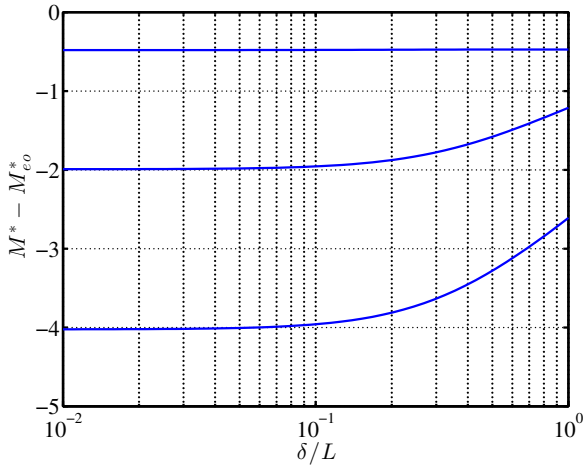

Fig. 8 Gel-electrophoretic mobilities with the same parameters as figure 6, but here varying δ/L with fixed $I_s = 10^{-3}$, 1, and 10^3 mM (increasing upwards).

3.4 Uncharged coronas with peripheral charge

The electrokinetic model is now applied to examine how the ionic strength of the bulk electrolyte impacts the electrophoretic mobility and drag coefficient of nanoparticles bearing terminally anchored ligands with charged end-groups. Following Hill et al.[14], the number densities of the Stokes resistance centers and charged end-groups are specified using Gaussian functions, as depicted in figure 10. These can model a variety of PEG ligands that have been used to functionalize gold and silver nanoparticles[10,11]. In

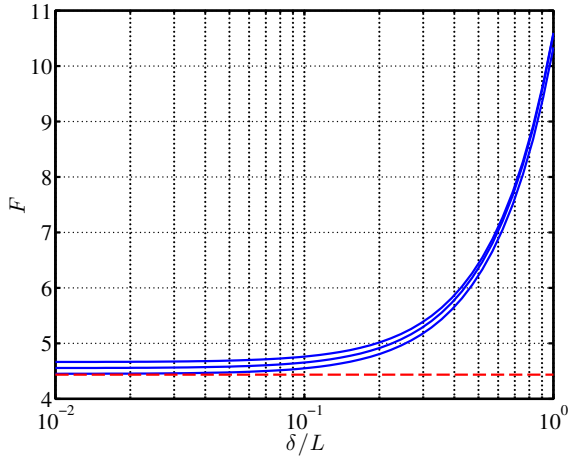

Fig. 9 Drag coefficients accompanying the mobilities in figure 8 (ionic strength increasing downward). Dashed line is the exact friction coefficient for a perfectly uniform, uncharged corona $\delta/L \to 0$ according to Hill and Li[13]. The offsets as $\delta \to 0$ reflect electroviscous effects, as highlighted in figure 6.

this paper, the Stokes-resistance-center density is

$$n_{s,c}(r) = n_{s,c,1} e^{-(r-L_1-a)^2/\delta_1^2} + n_{s,c,2} e^{-(r-L_2-a)^2/\delta_2^2} \tag{10}$$

with a fixed charge density (proportional to the second Stokes-resistance-center density)

$$\rho_{f,c}(r) = -e n_{f,c,2} e^{-(r-L_2-a)^2/\delta_2^2}. \tag{11}$$

Letting N_a denote the aggregation number, and N_s the number of Stokes resistance centers in a ligand, it follows that (taking $N_s \gg 1$)

$$N_s N_a = \int_a^\infty n_{s,c}(r) 4\pi r^2 \mathrm{d}r \approx 4\pi a^3 n_{s,c,1} f(\delta_1/a, L_1/a = 0)$$

and

$$N_c = \int_a^\infty n_{f,c}(r) 4\pi r^2 \mathrm{d}r = 4\pi a^3 n_{f,c,2} f(\delta_2/a, L_2/a),$$

where

$$f(x,y) = x^2 e^{-(y/x)^2}(y+2)/2 + x(1/2)\sqrt{\pi}(y^2+2y+x^2/2+1)[1+\mathrm{erf}(y/x)].$$

The number of end groups $N_c = N_a$, since each ligand is taken to bear one terminal resistance center with valence -1 from the dissociation of H^+. In this paper, all Stokes resistance centers are prescribed the same radius a_s.

Note that the Stokes-resistance-center density in Eqn. (10) is implemented within a much more general model framework by assigning the uncharged portion (with parameters $n_{s,c,1}$, L_1 and δ_1) to the Cl^- ion ($j = 2$ with zero fixed charge), and the charged portion (with parameters $n_{s,c,2}$, L_2 and δ_2) to the H^+ ion ($j = 1$).

The specific parameters adopted for the calculations presented below are as follows: $a = 2.7$ nm, $n_{s,c,1} \approx 19.8$ M, $L_1 = 0$ nm and $\delta_1 \approx 4.0$ nm; $n_{s,c,2} \approx 0.178$ M, $L_2 \approx 4.0$ nm and $\delta_2 \approx 1.33$ nm; $N_a = N_c \approx 146$, $N_s = 100$, and $a_s = 0.15$ Å, $\sigma = -1.5$ μC cm^{-2}. The net particle valence furnished by Eqn. (7) is $z \approx -154$; as to be expected, this agrees with the sum of the corona valence

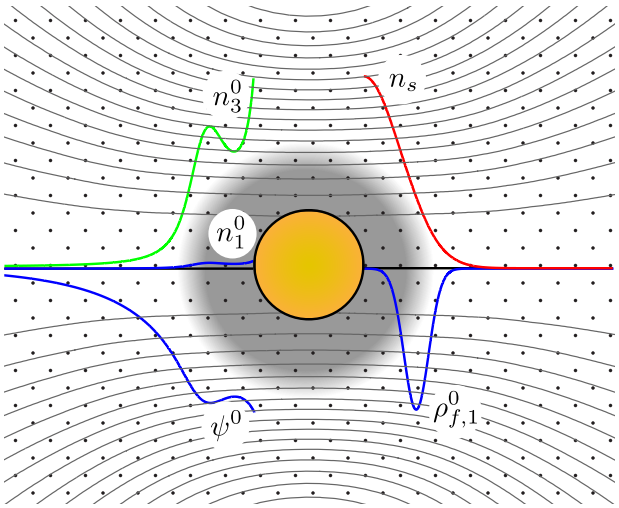

Fig. 10 Schematic of the core-corona architecture used to model functionalized nanoparticles (e.g., carboxymethylated-PEG grafted to a gold core) according to Eqns. (10) and (11). Here, negative charge is immobilized on the core surface (surface charge density σ) and in the corona periphery and gel (fixed charge density $\rho_f = \rho_{f,1}^0$ from the dissociation of H^+) with the corona segment density n_s decaying monotonically with distance from the core surface. Moreover, fixed charge comes from the dissociation of H^+ with the dominant ions within the corona (here at bulk ionic strength $I \sim 1$ mM) being H^+ (equilibrium concentration n_1^0) and Na^+ (equilibrium concentration n_3^0).

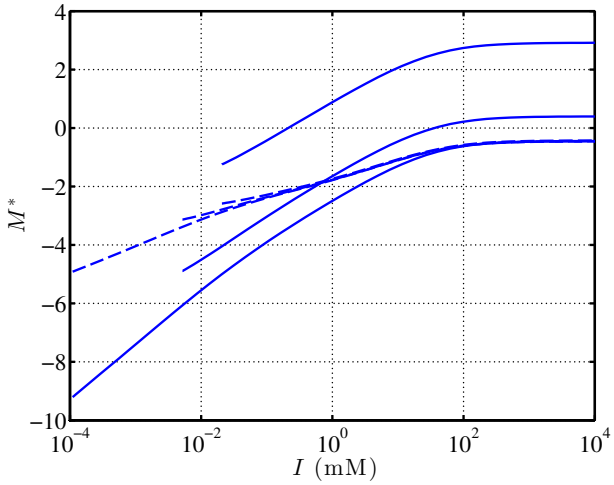

Fig. 11 Absolute gel-electrophoretic mobilities for core-corona nanoparticles in gels with charge densities $\rho_{f,g}^0 = 0, -1, -4$ kC m^{-3}. Solid (dashed) lines are for gels with high (low) permeability: $\ell_g^2 = 10^4$ or 10^2 nm^2. The lower limit of I for each curve identifies the ionic strength at vanishing added salt (10^{-7} M for uncharged gels containing pure water, and higher for charged gels containing pure water and counterions).

$-N_c = -146$ and the core valence $4\pi a^2\sigma/e \approx -8.6$.

The absolute gel-electrophoretic mobilities are shown in figure 11 for low- and high-permeability gels with three gel charge densities. For the low-permeability gels ($\ell_g = 10$ nm), the electroosmotic flow velocity is practically zero, and so the fixed charge density has a negligible influence on the particle mobility. For the high-permeability gels, however, the electroosmotic flow velocities in the gel are two orders of magnitude higher than in the low-permeability gels. This varies the particle mobilities in proportion to the fixed charge density (with fixed permeability). Note that the fixed charge on the gels is negative, which drives a positive electroosmotic flow in the opposite direction to the intrinsic/relative particle mobility.

The dimensionless equilibrium electrostatic potential at the core surface is shown in figure 12. This is somewhat higher than in figure 7. As depicted in figure 10, the magnitude of the equilibrium electrostatic potential has a local maximum in the corona periphery due to the fixed charge there. This peripheral charge clearly increases the potential at the core surface more than for the polyelectrolyte-coated particles in figure 7. This reflects a much higher, and more compact, corona charge. Recall, the valence of the polyelectrolyte-coated nanoparticles in figure 7 is $z \approx -68$, whereas the valence for the functionalized nanoparticles in figure 12 is $z \approx -154$.

The relative mobilities are shown in figure 13 with predictions of the mobilities at vanishing ionic strength according to Eqn. (6) with $z = -154$ from Eqn. (7), and $F = 3.5$ for the high-permeability gels ($\ell_g = 100$ nm) and $F = 6.5$ for the low-permeability gels ($\ell_g = 10$ nm). These drag coefficients are taken from plots of the exact drag coefficients F plotted in figure 14. The high-permeability gel furnishes a hydrodynamic radius $a_h \approx 3.5a \approx 9.5$ nm at high ionic strength, which increases by a factor $\approx 6.5/3.5 \approx 1.9$ when placed in the low-permeability gel.

Unlike the much more uniform polyelectrolyte coronas examined above, there is no independent theory available to predict these drag coefficients. Nevertheless, a simple approximation is to take the hydrodynamic radius in a pure electrolyte, $a_h \approx 3.5a$, which could be determined experimentally using dynamic light scattering, and to multiply by the Brinkman factor from Eqn. (4). Accordingly, for the gel with $\ell_g = 10$ nm, $F_B \approx 2.04$ furnishing a drag coefficient in the gel $F \approx 2.04 \times 3.5 = 7.1$, shown as the horizontal dashed line in figure 14. This clearly over-estimates the actual drag coefficient, but is still a very reasonable approximation given its straightforward calculation. The red dashed lines in figure 13 are the relative mobilities predicted from the high-permeability/free-solution mobilities ($\ell_g = 100$ nm) by dividing by the foregoing Brinkman factor ($F_B \approx 2.04$). Slightly better predictions (green dashed lines) are obtained by dividing the free-solution mobilities by the drag coefficient from the exact calculations, i.e., $6.5/3.5 \approx 1.9$. To obtain this factor experimentally, however, one must measure the hydrodynamic diffusion coefficient in a gel, which may be subject to steric influences.

A final point concerns the relaxation effects, which are evidently much weaker than suggested by many literature calculations for soft spheres undergoing free electrophoresis. The mobilities in figure 8 of Hill et al. [15], for example, exhibit much more significant influences of the polarization and relaxation phenomena. These mobility versus ionic strength relationships often exhibit an intermediate mobility minimum when $\kappa a \sim 1$, and all appear to increase monotonically with vanishing ionic strength. An explanation for the much weaker roles of polarization and relaxation for nanoparticle electrophoresis rests on two important factors: one is the net particle charge, and the other is the particle size.

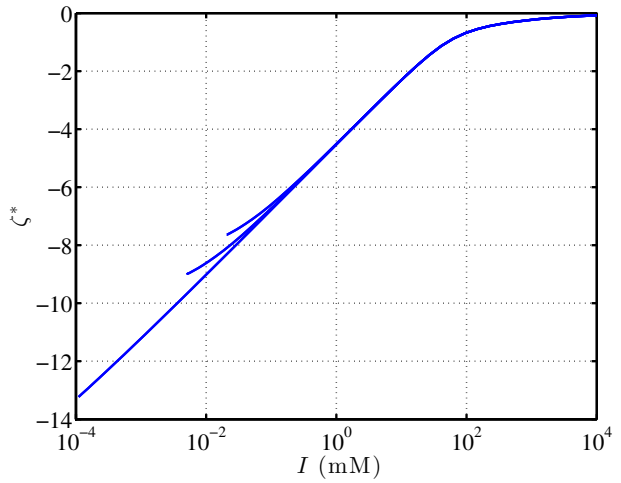

Fig. 12 Core surface ζ-potential for the core-corona nanoparticles in figure 11.

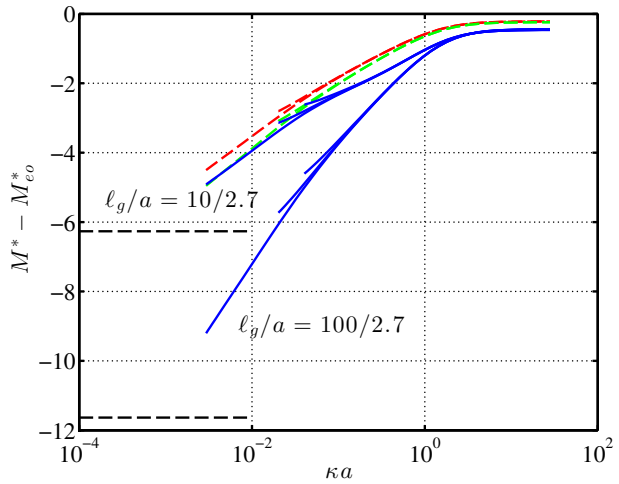

Fig. 13 Relative gel-electrophoretic mobilities for the core-corona nanoparticles in figure 11 (solid lines). Red dashed lines are obtained from the mobilities in high-permeability gels (relative mobilities approximately equal to the free-solution mobility) by dividing by the Brinkman factor $1+a_h/\ell_g+(a_h/\ell_g)^2/9 \approx 2.04$ (with $a_h \approx 3.5a$, see figure 14), whereas the green dashed lines are obtained by dividing the free-solution mobility by the actual drag coefficient $\approx 6.5/3.5 \approx 1.9$ (at high ionic strength, see figure 14). Horizontal lines are the Hückel mobilities furnished by Eqn. (6).

To better understand the polarization and relaxation influences, mobilities for the nanoparticles bearing coronas in figures 11–14 are compared in the top panel of figure 15 with and without the relaxation terms (ion-concentration perturbations); here in uncharged gels with low and high permeability. This clearly shows the polarization and relaxation effects manifesting when the ionic strength $I \lesssim 100$ mM, which coincides with the core surface potential ζ passing through ≈ -25 mV (right panel). For these very small nanoparticles (core radius $a_c = 2.7$ nm), the mobilities with and without the relaxation effects are qualitatively similar, increasing monotonically with decreasing ionic strength, in a similar manner to the surface potential.

The bottom panel of figure 15 shows the result of increasing the core radius by a factor of 16 ($a_c = 43.2$ nm), maintaining the same corona structure. Increasing the core radius by a factor of 16 increases the hydrodynamic size by a factor of approximately 16, and the surface area by a factor of $16^2 = 256$. The net valence is now $z \approx -39.5 \times 10^3$, which is indeed a factor 16^2 higher than for the smaller particles in the top panel. Now, despite the particles having the same surface charge density and corona architecture, the weaker surface curvature manifests in a slightly higher surface potential, but profoundly stronger relaxation effects. Without relaxation effects, the larger particles have higher mobility magnitudes at low ionic strength, since the net charge has increased by a factor 16^2 that is much larger than the increase in hydrodynamic size (in the high-permeability gels). In the low-permeability gel ($\ell_g = 10$ nm), the relaxation effects yield a mobility magnitude that decreases with decreasing ionic strength. Despite the high charge and electrostatic potential, the mobility is still predominantly a monotonic function of the ionic strength.

Removing the charged coronas from the particles in figure 15 furnishes the mobilities and core surface ζ-potentials shown in figure 16. Now the smallest particles ($a = 2.7$ nm) have a net charge that places the electrostatics mostly in the Debye-Hückel regime. The relaxation effects are now very weak with the mobilities at low ionic strength according to the Hückel limit Eqn. (6) ($M^* = \zeta^*$ in solution without gel), and the mobilities at high ionic strength according to the Smoluchowski limit ($M^* = 3\zeta^*/2$ in solution without gel). The large particles, despite having the same surface charge density, have a much higher surface ζ-potential at low ionic strength, and a lower ζ-potential at low ionic strength. These are also subject to very strong relaxation effects, with the particles in low- and high-permeability gels all having a local mobility magnitude maximum when $I \sim 1$ mM.

The free-solution mobilities (dashed lines) are also shown in the left panels of figure 15 according to the well-known Henry formula, which can be written

$$M^* = \zeta^* H(\kappa a) \quad (\zeta^* \ll 1), \tag{12}$$

where the Henry function $H(\kappa a)$ transits from 1 when $\kappa a \to 0$ to $3/2$ when $\kappa a \to \infty$. At very low ionic strengths, the Henry formula is in excellent agreement with the calculations for highly permeable gels without relaxation effects, but is a poor model for larger spheres at low ionic strengths, because the relaxation effects are significant. The the practical consequences of these observations are underlined below when applying the model to interpret gel-electrophoresis experiments performed on similarly sized nanoparticles in passivated agarose gels.

3.5 Passivated gel-electrophoresis: nanoparticles with pH charge-regulated surfaces

Zhu and Mason [28] recently separated polystyrene nanoparticles bearing different surface charge densities in passivated agarose gels, to which polyethylene glycol is added to prevent particle adhesion [27]. Here, the surface charge moieties are small enough for the particles to be considered bare spheres. With a radius $a \approx 42$ nm, and a buffer furnishing $\kappa a \approx 10$ (5 mM ionic strength, Debye length $\kappa^{-1} \approx 4.0$ nm), Zhu and Mason reported the mobility

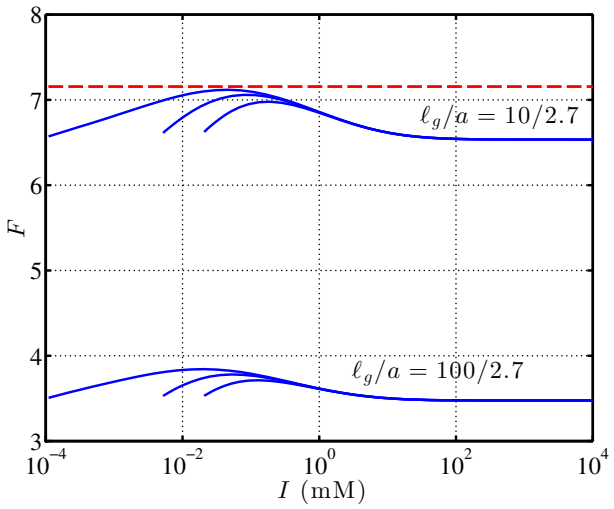

Fig. 14 Drag coefficient (force under translation at velocity V scaled with $-6\pi\eta aV$) for the core-corona nanoparticles in figure 11. In the high-permeability gel ($\ell_g = 100$ nm), $F \approx 3.5$ reflects the hydrodynamic contribution of the corona to the core ($a = 2.7$ nm). In the low-permeability gel ($\ell_g = 10$ nm), $F \approx 6.5$ reflects the additional viscous dissipation from hydrodynamic interaction with the gel (in the Brinkman approximation). The horizontal line is the product of the Brinkman factor $1 + a_h/\ell_g + (a_h/\ell_g)^2/9 \approx 2.04$ and $a_h/a \approx 3.5$ with $\ell_g = 10$ nm.

(at high pH where the particles are fully charged) to be -4.2×10^{-7} m^2 s^{-1} V^{-1}. When expressed as a dimensionless mobility, this is $M^* \approx -32$, which is extraordinarily high. As highlighted by Zhu and Mason, Palanisami and Miller [21] reported the free-solution mobility of larger polystyrene spheres (radius $a \approx 228$ nm) in buffer having ionic strength ≈ 63 mM (with pH ≈ 7.4) to be -3.07×10^{-8} m^2 s^{-1} V^{-1}, which is $M^* \approx -2.9$.

Zhu and Mason used the Hückel formula to convert their mobilities to a particle valence, which we have seen is questionable for highly charged particles at ionic strengths where (i) the diffuse double layer has a finite thickness, and (ii) polarization and relaxation effects are significant. Despite the potential pitfalls, the Hückel formula furnishes $z \approx -1900$ or $\sigma \approx -1.3$ μC cm^{-2}, which is physically acceptable and superficially compatible with literature. For example, studies that have carefully analyzed the free-solution electrophoretic mobilities of latex spheres [5], using the non-linear Poisson-Boltzmann equation and the theory of O'Brien and White [19] to account for relaxation effects, find surface charge densities 1–8 μC cm^{-2} (where 1 μC cm$^{-2} \approx 0.06e$ nm^{-2}). Thus, when interpreted using the Hückel formula, the surface charge density emerging from an anomalously high mobility appears to be physically acceptable. As demonstrated below, this reflects a cancellation of errors.

In an attempt to account for the finite thickness of the diffuse double layer (still neglecting relaxation effects), applying the Henry formula (with $\kappa a \approx 10$) to the mobility of the particles in Zhu and Mason's experiments furnishes $\zeta \approx -650$ mV, which leads to a surface charge density (from the LOW tables for $\kappa a > 0.5$, Russel et al. [24]) $\sigma \approx -8000e$ nm^{-2}. These are both extraordinarily high and physically unacceptable. On the other hand, the Henry formula (with $\kappa a \approx 190$) applied to the mobilities of the particles in Palanisami and Miller's experiments furnishes $\zeta \approx -50$ mV and (from LOW tables) $\sigma \approx -0.21e$ nm^{-2}, both of which are physically acceptable and compatible with the foregoing literature interpretations of free-solution mobilities.

Because Henry's formula neglects relaxation effects, calculations with the relaxation effects (e.g., furnishing the mobilities in the bottom panel of figure 16 at $I \approx 5$ mM) would demand even higher surface charge densities. Interestingly, the particles in Zhu and Mason's experiments are reported (by the manufacturer) to have approximately 6000 surface charge groups [28], so Zhu and Mason's estimate of the particle valence, -1900 (from the Hückel formula) would suggest incomplete deprotonation at the highest pH values where their mobilities (and by inference the charge/valence) plateau to limiting values.

To address the foregoing anomalies, let us now turn to an interpretation of Zhu and Mason's data using the present gel-electrophoresis model, which will account for the non-linear electrostatics (high charge), pH-regulation, and relaxation effects. The following interpretation is undertaken with an assumption that the mobilities of Zhu and Mason [28] are proportional to the measured velocities, but inversely proportional to an (unknown) electric-field strength that will be ascertained by fitting their reported velocities/mobilities to the theoretical model (via a constant scaling factor). Following Zhu and Mason [28], it will also be assumed that the electroendoosmotic flow in their gels is negligible.

The carboxylated polystyrene spheres with nominal radius $a = 42$ nm are reported to have $-z_0 \approx 6000$ carboxyl surface moieties. Thus, if these were fully dissociated (at high pH), the surface charge density $\sigma_0 \approx -0.271e$ nm$^{-2} \approx -4.34$ μC cm^{-2}. Note that the average charge separation is ≈ 1.9 nm, which is small, but still larger than the Bjerrum length (≈ 0.7 nm) so we might still expect to achieve complete deprotonation at high pH.

Zhu and Mason [28] interpreted their data assuming that the mobilities are proportional to a surface charge density that varies with the buffer pH according to an acid-dissociation model, furnishing

$$z = \frac{z_0}{1 + 10^{\mathrm{pK}_a - \mathrm{pH}}} \tag{13}$$

with $\mathrm{pK}_a = 4.6$ providing the best fit to their mobility data. This charging relationship is shown as the dashed line in figure 17(b).

To model a pH charge-regulating surface, a bare uncharged sphere is now endowed with a very thin pH charge-regulating polyelectrolyte surface layer. The radial distribution of carboxyl moieties is prescribed with a distribution of Stokes resistance centres

$$n_{s,c}(r) = n_{s,c,1} e^{-(r-a)^2/\delta^2} \tag{14}$$

with a fixed charge density

$$\rho_{f,c}(r) = \frac{-e n_{s,c}(r)}{1 + 10^{\mathrm{pK}_a(r) - \mathrm{pH}(r)}}. \tag{15}$$

While the charge-dissociation model is the same as adopted by Zhu and Mason, here it is applied locally, so $[\mathrm{H}^+](r) = 10^{-\mathrm{pH}(r)} = [\mathrm{H}^+]^\infty e^{-\psi(r)/k_B T}$ with $\psi(r)$ the local electrostatic potential and $[\mathrm{H}^+]^\infty$ the bulk hydronium concentration. Calculations reported in figure 17 have $\delta = 0.2$ nm and $a_s = 0.15$ Å, with $n_{s,c,1}$ in Eqn. (14)

according to

$$-z_0 = \int_a^\infty n_{s,c}(r) 4\pi r^2 \mathrm{d}r = 4\pi a^3 n_{s,c,1} f(\delta/a), \qquad (16)$$

where

$$f(x) = x^2 + x(\sqrt{\pi}/2)(x^2/2+1).$$

Note that the electrokinetic model should primarily reflect the net charge z_0, not details of the radial charge distribution, via the model parameters δ, a_s and $n_{s,c,1}$ in Eqn. (14). This was indeed verified to be the case (see the appendix for mobilities calculated with a more diffuse surface charge layer, $\delta = 1$ nm). With such a thin layer, the hydrodynamic resistance of the Stokes segments/fixed charge moieties is weak compared to the resistance from the no-slip surface to which these moieties are attached. This requires $\kappa\delta \lesssim 1$, which is readily verified to prevail here. Moreover, the bulk electrolyte contains a prescribed hydronium concentration $[\mathrm{H}^+]^\infty = 10^{-\mathrm{pH}}$ M with $[\mathrm{OH}^-]^\infty = 10^{-14+\mathrm{pH}}$; and $[\mathrm{Na}^+]^\infty$ and $[\mathrm{Cl}^-]^\infty$ are set to either $I_s = 5$ mM or the value that ensures bulk electroneutrality (according to whether the pH is greater or less than 7). It follows that the bulk ionic strength increases as the bulk pH deviates from 7.

As shown in figure 17, $\kappa a \approx 10$ with pH = 4–10, increasing to $\kappa a \approx 100$ at low and high pH. Figure 17(b) compares the particle valences according to Eqn. (13) and the non-linear Poisson-Boltzmann equation. This clearly demonstrates how the finite electrostatic potential at the particle surface increases the concentration of hydronium ions with respect to the bulk, therefore protonating a larger fraction of the carboxyl groups, reducing the valence. Accordingly, the effective pK_a is somewhat larger than the prescribed value ($\mathrm{pK}_a = 4.6$), e.g., $z/z_0 = 1/2$ when pH ≈ 6.

Figure 17(c) shows the surface potential according to the non-linear Poisson-Boltzmann equation. This increases with pH at low pH, because of the decreasing degree of potonation, reaching a maximum at pH ≈ 7. A further increase in pH continues to increase the surface charge, but this is accompanied by an increase in ionic strength, which decreases the surface potential (while maintaining a fixed charge). Also shown is the free-solution mobility for bare spheres according to the Henry formula (12) when assuming the ζ-potential equals the surface potential $\zeta^* = \psi^*(r=a)$ (reasonable when $\kappa\delta \approx 0.0048\kappa a \ll 1$).

Zhu and Mason assumed that $M^* \propto z$, which according to the Henry model ($M^* \propto \zeta^*$) implicitly demands $z \propto \zeta^*$, occuring only when $|\zeta^*| \lesssim 1$ and pH $\lesssim 4$. However, the Henry theory does not include relaxation effects or hydrodynamic interaction with the gel. Figure 17(d) shows mobilities with the relaxation effects for several uncharged/passivated gels having greatly varying permeabilities ($\ell_g = 10$–1000 nm). Whereas the free-solution Henry mobility reaches values as large as $M^* \approx -5$ at pH ≈ 9, the maximum free-solution mobility with relaxation effects is $M^* \approx -3.5$. Note that the Hückel limit in the fully charged state ($z = z_0 = -6000$) furnishes an extremely high mobility, $M^* \approx -102$ ($M = z_0 e/(6\pi\eta a) \approx -1.3\times10^{-6}$ m^2 s^{-1} V^{-1}). This is two orders of magnitude higher than predicted by the Henry formula with the ζ-potential prescribed by the non-linear Poisson-Boltzmann equation [dashed-dotted lines in figures 17(c) and (d)]. The Hückel mobility is also an order of magnitude larger than reported by Zhu and Mason.

The full calculations (solid lines) exhibit the same mobility versus pH relationship as measured by Zhu and Mason, albeit at pH values less than ≈ 10. At higher pH values (not achieved experimentally), the plateau mobility increases, because of an attenuation of the relaxation effects, bringing the mobilities closer to the Henry limit (dashed-dotted line). Also shown in figure 17(d) are the experimental data (circles) and model (dashed line) of Zhu and Mason. Note that these have been multiplied by a scaling factor that brings their plateau mobility (-1.85) into correspondence with the full theory with $\ell_g = 10$ nm (neglecting steric friction). Note that when scaled in this manner, the data and model are in excellent correspondence over the full range of pH.

The gel-electrophoretic model (applied here to data where steric effects are weak) captures very well the manner in which the gel-electrophoretic mobilities of Zhu and Mason change with respect to pH. However, there remains the question as to how the absolute mobility magnitudes reported by Zhu and Mason could be so large, thus requiring an arbitrary scaling factor correction. To this end, in a private communication, Professor Mason kindly advised that preliminary indications (based on measuring the electrical conductivity and considering the sample geometry) are that the electric-field strengths are likely $\approx 40\times$ higher than reported. This amounts to rescaling their reported mobilities by a factor $1/40 \approx 0.025$, thus bringing the plateau mobility in figure 17 (red dashed line) to $M^* \approx -2.6$ from the previously estimated $M^* \approx -1.85$. Without a steric force, the theory then suggests a gel permeability closer to $\ell_g \approx 20$ nm. Interestingly, allowing for a steric force (as an empirical fitting parameter) increases the permeability to a value that is closer to the free-solution electrophoresis limit achieved when $\ell_g \gtrsim 100$ nm. This seems plausible when considering the very low agarose concentration used in these experiments (0.6 wt%). For example, figure 6 of Zhu and Mason [27] suggests that the mesh size in such gels is ≈ 150 nm. Based on these considerations, figure 19 in the appendix compares the theoretical model with rescaled experimental mobilities when $\ell_g = 1000$ nm (mimicking free-solution electrophoresis). This clearly furnishes a satisfying fit, but now with a steric factor as the fitting parameter (steric friction force $\gamma = 0.2\times$ the hydrodynamic drag force) rather than the foregoing rescaling of the electric-field strength.

In future experimental studies, particular attention should be given to converting the applied voltage on the electrodes to the electric-field strength in the sample where the particle velocities are measured. Complementary measurements of particle mobilities in free solution would also be extremely beneficial, as the theory for free-electrophoresis is much better understood, as are the experimental methods. A concerted application of experiments and the electrokinetic model presented herein will hopefully enable steric influences to be isolated and theoretically modelled according to specific nanoparticle and gel architectures.

4 Conclusions

A comprehensive electrokinetic model has been developed for a very broad-class of spherical nanoparticles in gels. This model accommodates soft charged coronas with charge regulation, multi-

component electrolytes, and ion-concentration perturbations (often termed "relaxation" or "polarization and relaxation" effects). In this paper, the model was carefully tested by several direct comparisons to recent literature calculations, albeit for particles with core-shell architecture[2].

New results were presented for nanoparticles bearing coronas with inhomogeneous architectures, including those with peripheral charge, elucidating how the particle size and charge influence mobilities in gels with different permeabilities and charge densities. Several interesting physical insights were gained from mobilities at high and low ionic strengths: analogues of the well-known Hückel and Smoluchowski limits for free-solution electrophoresis of bare spheres.

Also identified was a small but finite relative mobility for uncharged bare spheres that depends on the particle dielectric constant when particles are dispersed in charged gels. Here, numerical calculations independently verified the theoretical prediction of Mohammadi and Hill[18], which furnished an exact analytical calculation of the electric-field induced force, including relaxation effects.

This paper also highlighted the important role of particle size (and thus charge) on the relaxation effects. Whereas these have often been attributed to the magnitudes of κa and ζ, it was demonstrated here that the relaxation effects can be assessed by reference to the particle charge (often scaling with the square of the radius). Thus, small nanoparticles with radii $\sim$ 1–10 nm tend to exhibit relatively weak relaxation effects, whereas relaxation effects for particles with radii $\gtrsim$ 10 nm exhibit much more substantial mobility attenuation by polarization.

A quantitative theoretical interpretation of the gel-electrophoretic mobilities of charge-regulating polystyrene spheres reported by Zhu and Mason[28] was undertaken. Particles were endowed a very thin charge-regulating polyelectrolyte surface layer. Accounting for relaxation effects, non-linear electrostatics, and hydrodynamic interaction with the gel, the theory furnished a mobility versus pH relationship that is remarkably close to the experiments in which steric friction is weak.

It was recommended that future experimental gel-electrophoresis studies pay special attention to the electric field, which depends on the electric current and sample/electrode geometry. Such studies will also benefit from reporting of free-solution mobilities in electrolytes having the same (or very similar) pH and ionic strength as in the gels (e.g., as indicated by the electrolyte and gel conductivities).

The theoretical model developed here is a powerful simulation tool. Free-solution mobilities can be now be interpreted separately, accounting for specific core-corona architectures. Then, gel-electrophoretic mobilities can be measured and theoretically interpreted to furnish deeper insights into the short-ranged and poorly understood nanoparticle-gel interactions.

5 Acknowledgements

Financial support from an NSERC Discovery Grant is greatfully acknowledged.

References

1 Adibnia, V., Hill, R. J., 2014. Electroacoustic Spectroscopy of Nanoparticle-Doped Hydrogels. Macromolecules 47 (22), 8064–8071.

2 Allison, S., Li, F., Le, M., 2016. Electrophoretic Mobility of a Dilute, Highly Charged "Soft" Spherical Particle in a Charged Hydrogel. J. Phys. Chem. B DOI: 10.1021/acs.jpcb.5b12224.

3 Allison, S. A., Xin, Y., Pei, H., 2007. Electrophoresis of spheres with uniform zeta potential in a gel modeled as an effective medium. J. Colloid Interface Sci. 313, 328–337.

4 Amsden, B., 1998. Solute diffusion within hydrogels. mechanisms and models. Macromolecules 31, 8382–8395.

5 Antonietti, M., Vorwerg, L., 1997. Examination of the atypical electrophoretic mobility behavior of charged colloids in the low salt region using the O'Brian-White theory. Colloid and Polymer Science 275 (9), 883–887.

6 Bhattacharyya, S., De, S., 2016. Gel electrophoresis and size selectivity of charged colloidal particles in a charged hydrogel medium. Chem. Eng. Sci. 141, 304–314.

7 Bhattacharyya, S., De, S., Gopmandal, P. P., 2014. Electrophoresis of a colloidal particle embedded in electrolyte saturated porous media. Chem. Eng. Sci. 118, 184–191.

8 Brinkman, H. C., 1947. A calculation of the viscous force exerted by a flowing fluid on a dense swarm of particles. Appl. Sci. Res. 1, 27–34.

9 Doane, T., Babar, A., Cheng, Y., Hill, R. J., Burda, C., 2010. Electrophoretic mobilities of pegylated gold NPs. J. Am. Chem. Soc. 132, 15624–15631.

10 Hanauer, M., Pierrat, S., Zins, I., Lotz, A., Sönnichsen, C., 2007. Separation of nanoparticles by gel electrophoresis according to size and shape. Nano Lett. 7, 2881–2885.

11 Hill, R. J., 2015. Corona charge regulation in nanoparticle electrophoresis. Proc. R. Soc. A 471, 20150522.

12 Hill, R. J., 2015. Hydrogel charge regulation and electrolyte ion-concentration perturbations in nanoparticle gel-electrophoresis. Proc. R. Soc. A 471, 20150523.

13 Hill, R. J., Li, F., 2013. Hydrodynamic drag coefficient for soft core-shell nanoparticles in hydrogels. Chem. Eng. Sci. 89, 1–9.

14 Hill, R. J., Li, F., Doane, T. L., Burda, C., 2015. Electrophoretic interpretation of PEGylated NP structure with and without peripheral charge. Langmuir 31 (37), 10246–10253.

15 Hill, R. J., Saville, D. A., Russel, W. B., 2003. Electrophoresis of spherical polyer-coated colloidal particles. J. Colloid Interface Sci. 258, 56–74.

16 Hill, R. J., Saville, D. A., Russel, W. B., 2003. Polarizability and complex conductivity of dilute suspensions of spherical colloidal particles with uncharged (neutral) coatings. J. Colloid Interface Sci. 268, 230–245.

17 Li, F., Allison, S. A., Hill, R. J., 2014. Nanoparticle gel electrophoresis: Soft spheres in polyelectrolyte hydrogels under the Debye–Hückel approximation. J. Colloid Interface Sci. 423 (0), 129 – 142.

18 Mohammadi, A., Hill, R. J., 2010. Steady electrical and microrheological response functions for uncharged colloidal inclu-

sions in polyelectrolyte hydrogels. Proc. R. Soc. A 466, 213–235.
19 O'Brien, R. W., White, L. R., 1978. Electrophoretic mobility of a spherical colloidal particle. J. Chem. Soc. Faraday Trans. 74, 1607–1626.
20 Ohshima, H. J., 1989. Approximate analytic expression for the electrophoretic mobility of colloidal particles with surface-charge layers. J. Colloid Interf. Sci. 130, 281–282.
21 Palanisami, A., Miller, J. H., 2010. Simultaneous sizing and electrophoretic mobility measurement of sub-micron particles using Brownian motion. Electrophoresis 31 (21), 3613–3618.
22 Phillips, R. J., 2000. A hydrodynamic model for hindered diffusion of proteins and micelles in hydrogels. Biophys. J. 79, 3350–3354.
23 Pons, T., Uyeda, H. T., Medintz, I. L., Mattoussi, H., 2006. Hydrodynamic dimensions, electrophoretic mobility, and stability of hydrophilic quantum dots. J. Phys. Chem. B 110, 20308–20316.
24 Russel, W. B., Saville, D. A., Schowalter, W. R., 1989. Colloidal Dispersions. Cambridge University Press, New York.
25 Waigh, T. A., 2016. Advances in the microrheology of complex fluids. Reports on Progress in Physics.
26 Wang, M., Hill, R. J., 2008. Electric-field-induced displacement of charged spherical colloids in compressible hydrogels. Soft Matter 4, 1048–1058.
27 Zhu, X., Mason, T. G., 2014. Passivated gel electrophoresis of charged nanospheres by light-scattering video tracking. J. Colloid Interface Sci. 428, 199–207.
28 Zhu, X., Mason, T. G., 2016. Separating nanoparticles by surface charge group using pH-controlled passivated gel electrophoresis. Soft Materials 14 (3), 1–6.

6 Appendix

This appendix comprises figures 18 and 19.

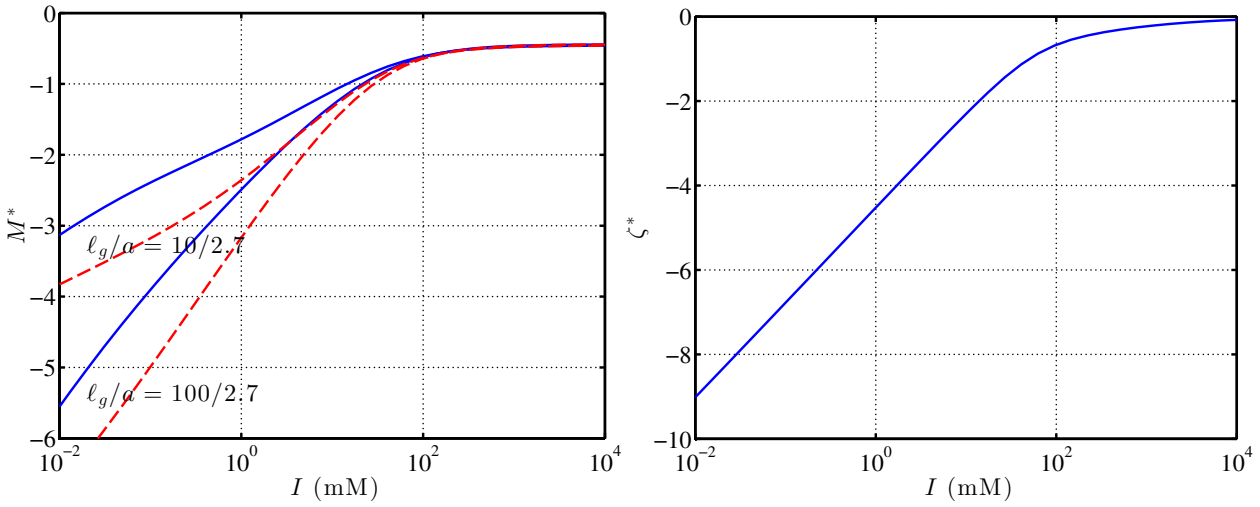

(a) $a = 2.7$ nm, $z \approx -154$

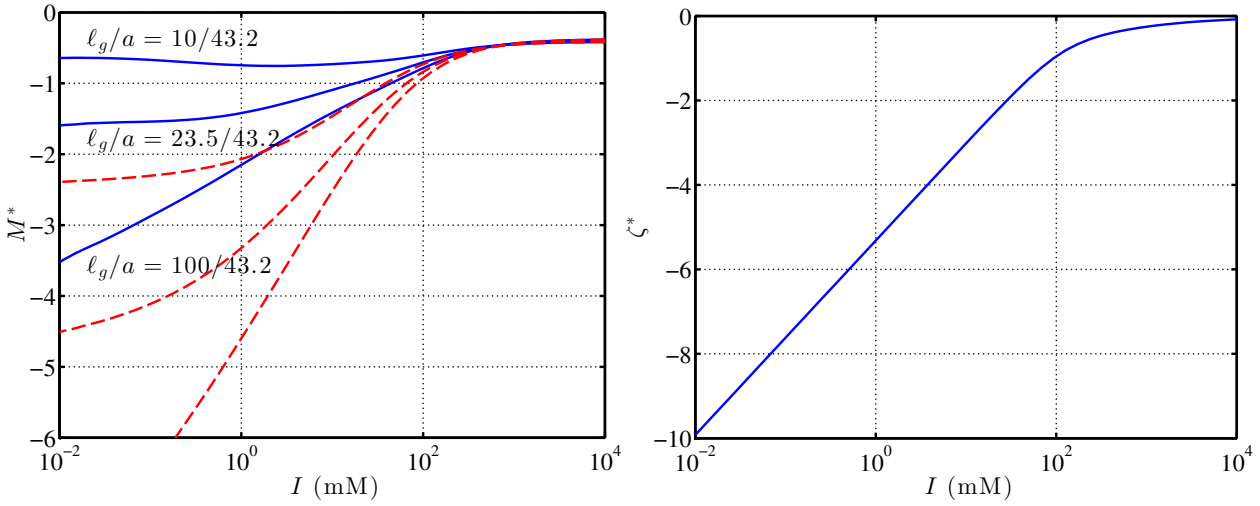

(b) $a = 43.2$ nm, $z \approx -39.5 \times 10^3$

Fig. 15 Gel-electrophoretic mobilities (left panels) and core surface ζ-potentials for core-corona nanoparticles in uncharged gels ($\rho^0_{f,g} = 0$ with $\ell_g = 10$, 23.5, 100 nm) highlighting the role of particle size on the relaxation effects: (a) $a = 2.7$ nm and (b) $a = 16 \times 2.7 = 43.2$ nm. Nanoparticles have the same surface charge density ($\sigma = -1.5$ μC cm^{-2}) and corona properties as in figures 11–14. Solid (dashed) lines are calculations with (without) the relaxation effects.

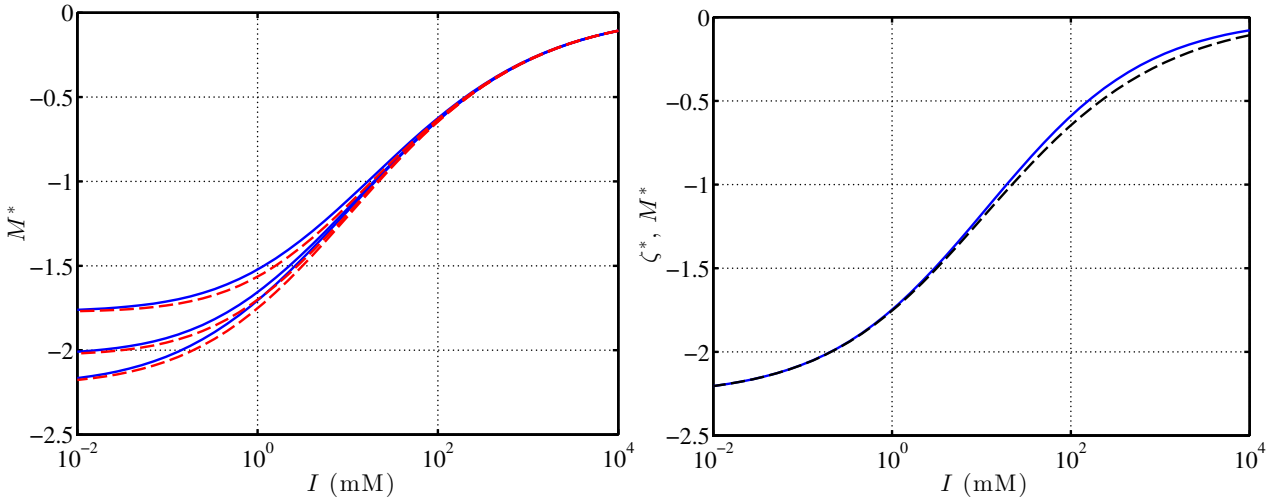

(a) $a = 2.7$ nm, $z \approx -8.6$ (bare spheres)

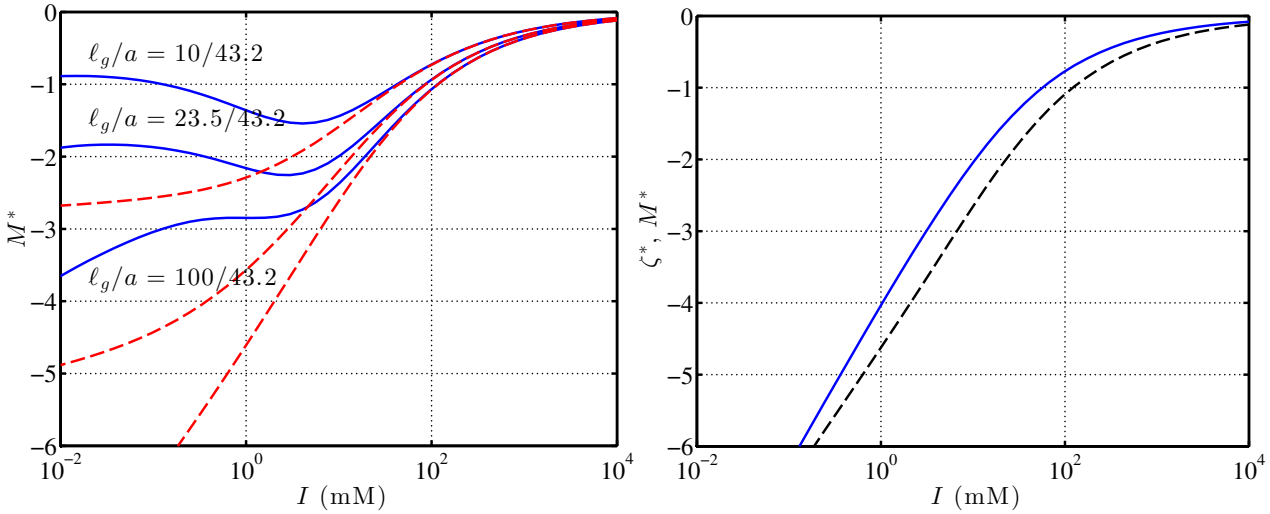

(b) $a = 43.2$ nm, $z \approx -2.2 \times 10^3$ (bare spheres)

Fig. 16 Gel-electrophoretic mobilities (left panels) and surface ζ-potentials (solid lines, right panels) for bare nanoparticles in uncharged gels ($\rho^0_{f,g} = 0$ with $\ell_g = 10,\ 23.5,\ 100$ nm) highlighting the role of particle size on the relaxation effects: $a = 2.7$ nm (a) and $a = 16 \times 2.7 = 43.2$ nm (b). Nanoparticles have the same surface charge density ($\sigma = -1.5\ \mu$C cm^{-2}) as in figures 11–14. In the left panels, solid (dashed) lines are calculations with (without) the relaxation effects. In the right panels, dashed-dotted lines are the Henry mobility obtained by multiplying the dimensionless ζ-potential (solid lines) by the Henry function $H(\kappa a)$.

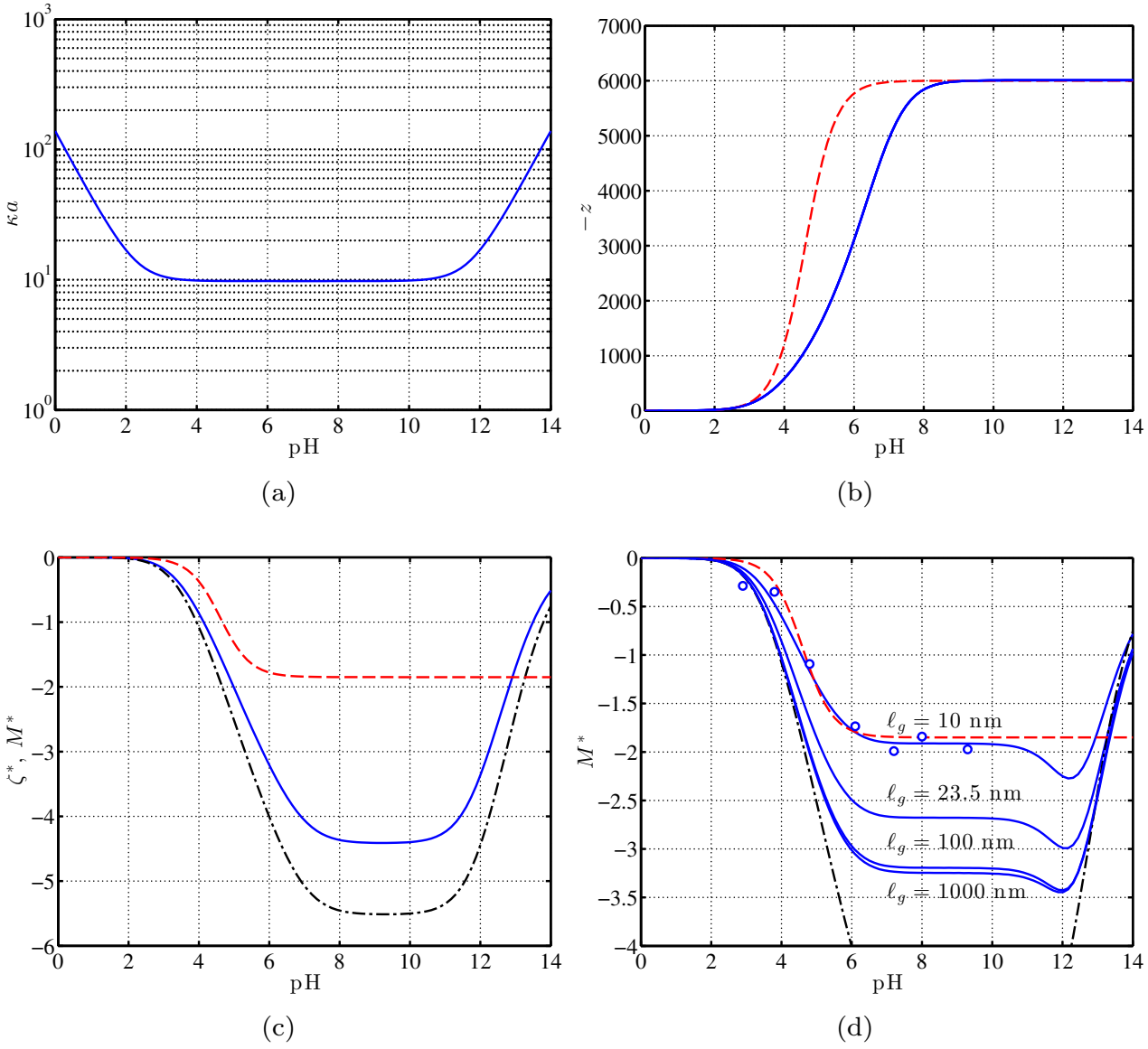

Fig. 17 Analysis of passivated gel-electrophoresis of carboxylated polystyrene nanoparticles (radius $a = 42$ nm) conducted in buffers with prescribed pH and $I_s = 5$ mM added salt (NaCl): $\mathrm{pK}_a = 4.6$, $z_0 = -6000$, $\delta = 0.2$ nm, $a_s = 0.15$ Å. (a) κa versus pH. (b) Particle valence z versus pH. Solid line is according to the non-linear Poisson-Boltzmann (PB) equation, and the dashed line is according to the dissociation equilibrium Eqn. (13) of Zhu and Mason [28]. (c) Solid line is the surface ζ-potential according to the non-linear PB equation. Dashed line is the free-solution mobility according to the Hückel formula $M = ze/(6\pi\eta a)$ with z according to Eqn. (13), but multiplied by an arbitrary scaling factor ($1.85/102 \approx 0.018$, see the main text for details on this rescaling). Dashed-dotted line is the free-solution mobility according to the Henry equation with ζ-potential according to the PB equation (solid line). (d) Solid lines are mobilities according to the full-electrokinetic model with gel permeabilities $\ell_g = 10$, 23.5, 100 and 1000 nm. Dashed-dotted line is the Henry mobility, as also shown in panel (c). Circles are experimental mobilities from Zhu and Mason [28] [rescaled as in panel (c)]. Dashed line is the mobility according to the phenomenological model of Zhu and Mason [28] [mobility proportional to valence from Eqn.(13)].

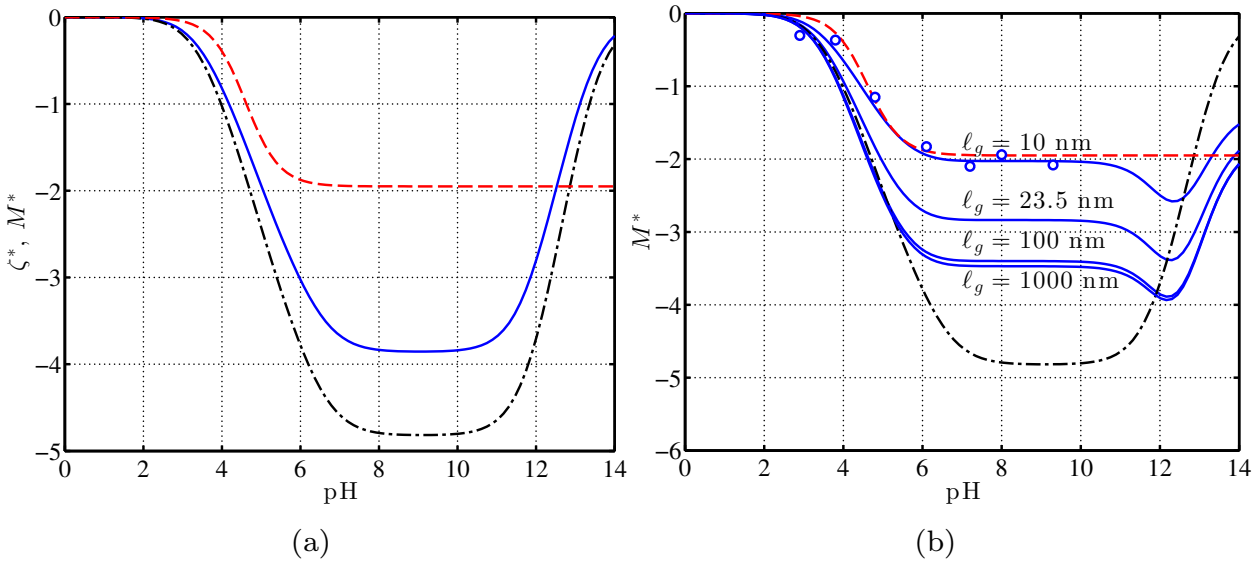

Fig. 18 The same as figures 17(b) and (c), but with a more diffuse surface charge layer, $\delta = 1$ nm. The most significant changes occur at high pH, when the surface charge density is high and the ionic strength is high enough to achieve $\kappa\delta = 0.024\kappa a \sim 1$ at very high pH.

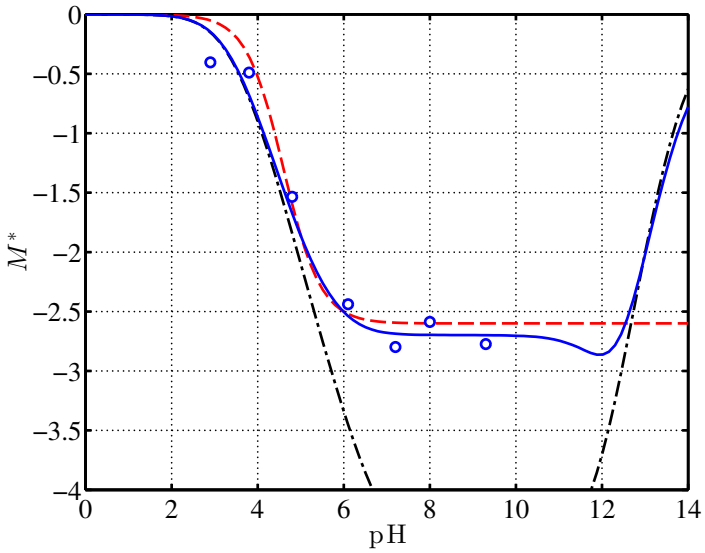

Fig. 19 Theoretical interpretation of the gel-electrophoretic mobilities reported by Zhu and Mason [28] when taking the electric-field strength to be a factor of $40\times$ higher than reported (mobilities a factor $40\times$ smaller than reported). Model parameters are the same as in figure 17(c), but here $\ell_g = 1000$ nm (mimicking the free-solution mobility) with a steric factor $1/(1+0.2) \approx 0.83$ (i.e., the steric drag force is $0.2\times$ the hydrodynamic drag force) as an adjustable model parameter. Dashed line is the mobility according to the phenomenological model of Zhu and Mason [28] [mobility proportional to valence from Eqn.(13)] (with the same correction to the electric-field strength as applied to the data). Dashed-dotted line is the free-solution mobility according to the Henry equation, but now with a steric factor $1/(1+0.2) \approx 0.83$.